Archaeomagnetic Dating of Bronze Age Pottery from Tell Mozan, Syria

A Thesis
Submitted to the Faculty of the Graduate School
of the University of Minnesota

By

Michele D. Stillinger

In Partial Fulfillment of the Requirements
for the Degree of Master of Arts

Katherine F. Hayes
Ellery Frahm

April 2013

Acknowledgements

This thesis research would not have been possible without the support of the following individuals and institutions. I would like to thank my Co-Advisor, Dr. Ellery Frahm, who introduced me to the field of geoarchaeology and provided me with both the materials and topic for this research. His support and encouragement kept me motivated while achieving my academic goals. He has been a true mentor, colleague and friend.

I am also grateful to my Advisor, Professor Joshua M. Feinberg, co-director of the Institute for Rock Magnetism (IRM), who was integral to the entire research process. Dr. Feinberg's guidance and enthusiasm have inspired me to reach higher and continue on in the field of geoarchaeology. Without his support this research would not have been possible.

The majority of this research was conducted in association with the Institute of Rock Magnetism at the University of Minnesota, therefore, I would like to thank Professor Bruce Moskowitz, director of the IRM, Research Associate Julie Bowles, and Research Professor Mike Jackson. The technical support of Mike and Julie throughout the entire process of equipment training, testing and analysis was invaluable and gratefully appreciated.

I would also like to thank the Evolutionary Anthropology Labs at the University of Minnesota for the use of the Leica microscopic and photographic equipment; the Geological Society of America's Archaeological Division for their support of this research in the form of the Richard Hay Student Poster Award in 2011; Georgio Buccellati and Marilyn Kelly-Buccellati, directors of the Tell Mozan excavation; and the Syrian Directorate General of Antiquities and Museums for approving the export of Tell Mozan artifacts.

Finally, I would like to thank my parents, family and friends for their continued support and encouragement. Thank you for being with me on this new chapter in my life.

Abstract

The ancient city-state of Urkesh, located at Tell Mozan, Syria, was the political and religious center of the Hurrians, a unique culture that inhabited the northern Syro-Mesopotamian region during the 3rd millennium BCE. The chronology of Urkesh has been divided into seven primary occupational phases, dating from the Early Dynastic II period (2800-2500 BCE) to the Middle Babylonian/ Mitanni Period (1500-1300 BCE). The site has provided an abundance of distinguishing ceramics, seals, seal impressions, and cuneiform tablets, which serve as the foundation for the Urkesh chronology.

Working under the assumption that the archaeologically derived chronology at Mozan was reliable, this research tested the accuracy of archaeomagnetic dating using pottery samples from six successive occupational phases. Samples underwent a suite of magnetic mineral characterization tests and archaeointensity measurements using the Thellier-style absolute paleointensity technique of Tauxe and Staudigel (2004). Archaeointensity experiments displayed an 88% success rate and 80% of the samples correlated well with their archaeologically determined dates. A small subset of samples appeared to indicate a possible intensity spike occurring around 2000 BCE. The final results refine the archaeointensity curve for Syria between 2350 and 1200 BCE.

Table of Contents

Acknowledgments i

Abstract ii

Table of Contents iii

List of Tables v

List of Figures vi

Introduction 1

Section 1: Geophysical Basis of Archaeomagnetism 4

1.1 Introduction to Archaeomagnetism 4

1.2 Geomagnetism 6

1.3 Rock Magnetism 7

1.3.1 Ferromagnetism 8

1.3.2 Magnetic Susceptibility 10

1.3.3 Magnetic Domain Structure 10

1.3.4 Remanence Anisotropy 11

1.3.5 Hysteresis 13

1.4 Paleomagnetism & Archaeomagnetism 16

1.5 Applications of Archaeomagnetism 18

Section 2: Previous Archaeomagnetic Research 20

2.1 Addressing Methodological Accuracy 20

2.2 Narrowing Data Scatter 22

2.3 Refining the Methodology 23

2.4 Previous Research in Syria 27

Section 3: Site Description 31

Section 4: Methods 36

4.1 Sample Selection and Preparation 36

4.2 Magnetic Measurements 42

4.2.1 Susceptibility and Superparamagnetism 42

4.2.2 Hysteresis 43
4.2.3 Alternating Field (AF) Demagnetization 44
4.2.4 AF Demagnetization of 1 Tesla IRM 45
4.2.5 Remanence Anisotropy 46
4.2.6 Thermal Remanent Demagnetization 46
Section 5: Results 48
5.1 Susceptibility and Superparamagnetism Results 48
5.2 Hysteresis and Domain Structure Results 49
5.3 AF Demagnetization Results 54
5.4 Thermal Remanent Demagnetization Results 59
5.5 Archaeointensity and Anisotropy Results 62
Section 6: Discussion 65
6.1 Construction of Preliminary Archaeointensity Dating Curve 65
6.2 Estimated Age of Samples of Unknown Archaeological Age 67
6.3 Preliminary Archaeointensity Dates for Samples of Known Archaeological Age 70
6.4 Comparison of Mozan Results to Greater Regional Curve 72
6.5 Comparison of Relative and Archaeomagnetic Dates for Mozan 74
6.6 Final New Archaeointensity Dating Curve for Syria 75
6.7 Sources of Dating Discrepancies 77
Section 7: Conclusion 79
References: 82
Appendix A: Sample Selection and Photos 87
Appendix B: All Sample Results and Curve Construction Parameters 94

List of Tables

Table 1. General Chronology of Urkesh and Associated Archaeological Periods 34
Table 2. Tell Mozan Pottery Samples 38
Table 3. Susceptibility Results 49
Table 4. Hysteresis Results 50
Table 5. Archaeointensity Results 63
Table 6. Comparison of Relative and Archaeomagnetic Dates for Tell Mozan 75
Table A1. Details of Pottery Sample Selection 87
Table B1. Results of Susceptibility, Hysteresis and AF Demagnetization 94
Table B2. Details from Intensity Experiments and Acceptance Test Results 96
Table B3. Intensity and ARM Results 97
Table B4. Polynomials Used in Construction of Intensity Curves 97

List of Figures

Figure 1. Generalized Hysteresis Loop 15
Figure 2. Magnetic Intensity for Syria 27
Figure 3. Location of Tell Mozan, Syria 32
Figure 4. Plan of Royal Palace Excavation 35
Figure 5. Representative Samples 40
Figure 6. Representative Specimens 42
Figure 7. Representative Hysteresis Loops 51
Figure 8. Domain States for All Samples 53
Figure 9. Representative AF Demagnetization Results 57
Figure 10. Representative Thermal Demagnetization Results 60
Figure 11. Preliminary Archaeointensity Curve for Syria 67
Figure 12. Mozan Data in Comparison to Preliminary Curve 69
Figure 13. Greater Regional Archaeointensity Dating Curve 73
Figure 14. New Archaeointensity Dating Curve for Syria 76
Figure A1. Photos of All Samples Prior to Preparation 89

Introduction

One of the fundamental requirements of any detailed archaeological investigation is a basic understanding of the occupational chronology at the site. In the absence of indisputable historical documentation, archaeologists have turned to relative and absolute dating techniques, which utilize material remains or geological indicators. In the Near East, the dating of ancient sites has traditionally relied on chronologies derived from ceramic seriation and more recently on radiocarbon analysis. Recent debate as to the precision of chronologies that rely solely on these two dating methods has resulted in a demand for the incorporation of an additional absolute dating tool in archaeological research. This study intends to test the precision of archaeomagnetic dating as an absolute dating technique. Archaeomagnetic dating, a subfield of paleomagnetism, is a geophysical technique that measures the record of the Earth's ancient magnetic field stored within archaeological materials. Archaeomagnetism can be used to construct field variation curves that function similar to the radiocarbon dating curve. These variation curves can then be used to date artifacts and sites, potentially down to an accuracy of ± twenty years.

Archaeomagnetic experiments in this study were conducted using pottery samples obtained from successive stratigraphic layers at the archaeological site of Tell Mozan, in northeastern Syria. Tell Mozan contains evidence of human occupation dating back to the Halaf Period (6^{th} millennia BCE) and has been identified as the location of the ancient city-state of Urkesh. Archaeologists have divided the Urkesh chronology into seven

notable occupational phases ranging from the Early Dynastic II period (circa 2800-2500 BCE) to the Babylonian/Mitanni period (circa 1500-1300 BCE) (Buccellati, 2003). The chronology at Tell Mozan is based on two primary sources: 1) textual and glyptic evidence, in the form of cuneiform tablets, inscribed seals, thousands of seal impressions, and ancillary historical documentation; and 2) an abundance of distinguishing ceramics used in ceramic seriation. This combination of textual evidence and well-dated ceramics offers an ideal archaeological control for investigating the application of archaeomagnetic dating as an absolute dating technique.

This study reports the results of a suite of magnetic mineral characterization tests and archaeomagnetic experiments. Magnetic intensity results from this study will be compared to previous archaeointensity data for Syria and the surrounding region and used (i) to augment and improve existing global and regional archaeomagnetic databases; (ii) to date samples from the site missing dates or from mixed stratigraphic context; and (iii) to determine the presence or absence of geomagnetic spikes, which are characterized as abrupt and unusually high increases in magnetic field intensity spanning a short time period, and could be used as distinguishing markers on archaeointensity dating curves (Gallet et al., 2006, Shaar et al, 2011). In addition, the results from this study will be used to determine the suitability of certain types of ceramics for archaeomagnetic dating, thus guiding sample selection in future research.

The archaeomagnetic research herein incorporates data acquisition and analysis techniques associated with the three sub-disciplines of geophysics: geomagnetism, rock magnetism, and paleomagnetism; therefore, a general overview of each field along with

definitions of terminology is discussed in Section 1 followed by a brief summary of the applications of archaeomagnetism relevant to archaeological research. An overview of the historical development of archaeomagnetism, previous research as it pertains to the development of secular variation dating curves, and archaeomagnetic research for Syria is summarized in Section 2. The Tell Mozan archaeological site is described in Section 3, followed by methods, results, discussion, and conclusion (Sections 4-7). Detailed sample analysis tables and photographs can be found in Appendix A. Complete archaeomagnetic data results for each specimen can be found in Appendix B.

Section 1. Geophysical Basis of Archaeomagnetism

1.1 Introduction to Archaeomagnetism

Archaeomagnetism, the study of the magnetic properties of archaeological materials, is a subfield of paleomagnetism, the study of the Earth's magnetic field direction and intensity recorded in volcanic and igneous rocks, soils, and sediments. The Earth's magnetic field is dynamic, from small daily fluctuations to complete polarity reversals that occur at frequencies of 100,000 years or more. Under the right circumstances, such as exposure to high temperatures, these variations in the magnetic field can be permanently recorded in materials that contain magnetic minerals. This process, called remanent magnetization, was first proposed in 1848 by Joseph Fournet, and experimentally identified in rocks and lava by Achille Joseph Delesse in 1849 and Macedonio Melloni around 1853. Both Delesse and Melloni discovered that rocks cooled in the presence of the Earth's field acquired a magnetization parallel to that field (Courtillot and Le Mouël, 2006). Between 1895 and 1900, Giuseppe Folgheraiter (the "father" of the field of archaeomagnetism) examined remanent magnetization using fired clay, bricks from Roman walls, and ancient Greek and Etruscan pottery, identifying the stability of magnetization held by these types of objects (Courtillot and Le Mouël, 2006).

Paleomagnetic investigation by Bernard Brunhes and Pierre David in the early 1900s recognized that remanent magnetization could be induced by a number of external sources including lightning, baking, and deep burial for thousands of years. They also

identified that the Earth's magnetic field reversed (Courtillot and Le Mouël, 2006). Additional research into field reversals was conducted by Matuyama in 1929. These experiments became the basis of one of the fundamental achievements of the paleomagnetic community, the development of the geomagnetic polarity timescale (GPTS), a chronologic record of all the geomagnetic reversals over the last 180 million years (Ma). The GPTS is used as a relative dating tool by stratigraphers, volcanologists, anthropologists, paleontologists, archaeologists, petroleum exploration scientists, and other scientific professions. These early investigations into magnetic remanence demonstrated that magnetization could be recorded in materials containing magnetic minerals, that the Earth's field changed through time and that this ancient remanence could be measured in the laboratory.

While the GPTS records the average, global field variation, archaeomagnetic research is concerned with investigating secular variations in the magnetic field, small fluctuations that are strongly dependent on location and time. Holocene secular variation patterns have been obtained through direct measurement of the magnetic field since the early 1600s (CE) and indirectly through studies of archaeological materials, volcanic rocks, marine sediment cores, and postglacial lake sediments (Butler, 1992). In the 1930s, the husband and wife team of Emile and Odette Thellier expanded the field of archaeomagnetism by developing new sampling and measurement techniques which improved accuracy and reduced laboratory measurement time (Courtillot and Le Mouël, 2006). By the 1940s, the Thelliers had introduced the technique of thermal demagnetization, the standard tool of archaeomagnetic and paleomagnetic research still

today. This method can be used to determine past field intensities recorded in archaeological materials. The Thelliers used the results of their archaeomagnetic research to publish the very first secular variation curves, graphs of field variation through time. Since the 1950s, archaeomagnetic research has focused on identifying magnetic variation during recent human history, primarily within the last 5,000 years, and using these secular variations to construct curves that can be used for dating ancient materials.

1.2 Geomagnetism

Archaeomagnetism incorporates analysis techniques from three geophysical fields of research: geomagnetism, rock magnetism, and paleomagnetism. Geomagnetism is the study of the origin, morphology and variation in the Earth's magnetic field (Sternberg, 1990). The Earth's magnetic field at a specific point on the surface is described by a vector composed of two directional components (declination and inclination) and a magnetic strength component (intensity). Declination is the horizontal angle in degrees between the measured magnetic field and geographic north. Inclination is the vertical dip in degrees from the horizontal, where downward dips are noted as positive. Field intensity is the magnitude of the vector total expressed in Teslas (T) (Sternberg, 1990).

Surface contour maps of the Earth's magnetic field indicate that it acts similar to a giant, geocentric axial dipole magnet, aligned nearly parallel with the rotational axis of the Earth (Butler, 1992; Sternberg, 1990). This best-fitting or 'eccentric' dipole accounts

for 90% of the Earth's surface magnetic field. While the eccentric dipole describes the geomagnetic field perfectly at many locations, at other locations there is still as much as a 20% discrepancy (Butler, 1992). This is due to the presence of non-dipolar field components, which are quantified as the difference between the observed geomagnetic field and the theoretical model of an eccentric dipole (Butler, 1992; Sternberg, 1990). Butler (1992) notes that non-dipolar features are spatially dynamic and are likely to be the result of fluid and convection currents in the liquid iron outer core.

The combination of dipole and non-dipole field components results in highly variable patterns of declination, inclination, and intensity across the Earth's surface; (Butler, 1992; Sternberg, 1990). Because of the non-linear variability of these parameters, archaeomagnetic dating requires the compilation of regionally specific geomagnetic field databases. For example, Sternberg (1990) estimates that for a directional measurement with 5° accuracy, a specific secular variation master record for a region is only useful out to a maximum of 2,000 km from the source of measurement. Most researchers, however, prefer to limit their secular variation curves to a specific country, or region no more than 1,000 km in size (Genevey et al., 2003).

1.3 Rock Magnetism

In order for remanent magnetization to be stored within rock and other materials, they must contain iron-rich ferromagnetic minerals, such as magnetite, hematite and titanomagnetite (Butler, 1992). These minerals frequently contain traces of titanium,

aluminum, chromium, and nickel, which can moderate the minerals' magnetic recording properties. Rock magnetism is the geophysical study of magnetic mineralogy, susceptibility, grain size distribution and arrangement of mineral assemblages. Researchers use these parameters to understand how a sample becomes magnetized and how it was originally formed. Rock magnetism aids in archaeomagnetic studies by identifying the specific magnetic carrier of remanence, which in turn can be used to identify the theoretical properties of those magnetic grains, such as preferential alignment and magnetic domain structure (Sternberg, 2001).

1.3.1 Ferromagnetism

Magnetization in ferromagnetic minerals is produced through electron-spin exchange coupling of adjacent atomic magnetic moments and is dependent on crystallographic structure of the mineral (Dunlop and Özdemir, 1997; Butler, 1992). Ferromagnetic minerals have the ability to become strongly magnetized and produce a spontaneous or saturation magnetization (Ms) at room temperature, even when exposed to a weak magnetic field. Each ferromagnetic material has a maximum saturation magnetization that decreases in a characteristic manner as the material is heated. When the material reaches its Curie temperature (T_C), the directions of the magnetic moments in the material become thermally disordered and the net magnetization is zero. For example, the Curie temperature for pure magnetite and hematite are 580°C and 680°C, respectively (Dunlop & Özdemir, 1997; Butler, 1992), distinctive temperatures that allow

for laboratory identification of magnetic mineralogy. As the material is cooled below the Curie temperature the net magnetization aligns parallel to the magnetic field. When the material cools below the magnetic blocking temperature (T_B), the magnetization becomes stable or "locked-in". This process results in the acquisition of a thermal remanent magnetization (TRM), which is the magnetization acquired during cooling after a material is heated above the Curie temperature of its constituent magnetic particles in the presence of an external magnetic field (Sternberg, 1990). Between the Curie and blocking temperatures, ferromagnetic grains behave like an assemblage of superparamagnetic grains, which are magnetic grains that can individually maintain a strong net magnetization, but collectively lose their magnetization when a magnetic field is removed (Butler, 1992). The magnetic relaxation time and blocking temperature are important to understanding the acquisition of remanent magnetization. Relaxation time is dependent on temperature, grain volume, and coercive force (a measure of the energy barrier to magnetic rotation). Blocking temperature is dependent on magnetic grain size and shape. Geological and archaeological materials can hold remanent magnetizations for billions of years in the absence of a reheating episode or induced magnetization, such as a lightning strike.

The rate at which a sample is cooled through its blocking temperature after an original heating episode is often slower than the cooling rate experienced in laboratory thermal testing. This difference in cooling rate is important because faster cooling rates in the lab usually produce lower TRM intensities for samples dominated by single domain grains (*see section 1.3.3*). For example, Chauvin et al. (2000) found that TRMs

of baked clays were 5-12% higher after slow cooling; however, Genevey et al. (2003) found no appreciable difference between laboratory cooling rates of 5, 10 and 20 hours, noting that different mineralogies and grain size distributions may play a greater role in the overall cooling rate effect.

1.3.2 Magnetic Susceptibility

Magnetic susceptibility (χ) is the induced magnetic response of a material to an externally applied field. Provided the applied field is small, the resulting induced magnetization will disappear immediately after the external field is removed, resulting in specimens that remain both physically and magnetically unaltered (Yu, 1990). Susceptibility is a unit-less value and is a measure of the ability or ease with which a substance becomes magnetized. Susceptibility measurements can be normalized by mass (reported as m^3kg^{-1}) in order to make a more meaningful comparison between samples of different sizes. The magnetic susceptibility of a specimen is frequently interpreted as a proxy for the concentration of magnetic minerals present. By measuring χ as a function of temperature it is possible to quickly determine a specimen's Curie temperature.

1.3.3 Magnetic Domain Structure

The concept of magnetic domains is fundamentally related to the size and shape of magnetic grains. Magnetic domains are uniformly magnetized regions within an

individual ferromagnetic grain that form in order to minimize magnetostatic energy (Butler, 1992). There are four broad categories of domain structures: superparamagnetic (SP), single domain (SD), pseudo-single domain (PSD), and multi-domain (MD). As grain size decreases, the number of domains also decreases and magnetostatic energy increases; thus, single domain grains are more efficient at carrying a remanent magnetization (Butler, 1992). The magnetizations of multiple domains within a single grain tend to cancel one another out, which means that MD grains are poor recorders of the Earth's magnetic field. In some cases, grains that are extremely small will be thermally excited even at room temperature and their magnetic moments will fluctuate on timescales of nanoseconds to minutes. These superparamagnetic (SP) grains are highly susceptible to field and temperature changes and do not hold a remanence over archaeological timescales. SD grains occur in most natural materials but represent only a small fraction of the total magnetic mineral assemblage. While SD grains are optimal for paleomagnetic studies, most magnetic grains fall between the SD and MD size range, called PSD grains, and often exhibit SD-like properties, which make them suitable for archaeomagnetic testing.

1.3.4 Remanence Anisotropy

Remanence anisotropy is the result of the preference of magnetic grains to align their magnetizations along their easy crystalline axes (magnetocrystalline anisotropy), or along their longest axes (shape anisotropy). These preferential forms of alignment

produce a magnetic barrier to rotation away from the easy or long axis, which must be overcome by an applied field. Without this energy barrier, remanence would not exist and magnetization would have a simple linear relationship with the applied field. Remanence anisotropy is influenced by many factors including magnetic grain size and shape, crystalline structure, domain structure, stress, and exchange coupling. If unrecognized, anisotropy can cause systematic errors in susceptibility and remanent magnetization measurements (Dunlop and Özdemir, 1997; Butler, 1992).

Archaeological ceramics, bricks and tiles, can also be highly anisotropic because of the nature of their fabrication. For example, in wheel-thrown pottery, the clay is smooth and pressed together along tightly bound parallel planes. The clay platelets are pressed together along their grain boundaries creating a material characterized by a strong mineral alignment (Chauvin et al., 2000; Rice, 2005). This alignment can have an effect on the accuracy of the magnetization acquired by the material as it cools through its blocking temperature resulting in a final remanence direction that is not oriented parallel to the applied field but is instead biased towards the plane of the mineral fabric. Archaeomagnetic tests by Kovacheva et al. (2000) found that ceramics have a higher anisotropy than bricks, which are usually formed by pounding clay into a mold.

Magnetic anisotropy can be quantified and corrected using either anisotropy of magnetic susceptibility (AMS) or anhysteretic remanent magnetization (AARM) (Butler, 1992; Dunlop and Özdemir, 1997; Tema 2009). An ARM is applied to a sample by simultaneously exposing a specimen to a small direct current (DC) field and a slowly decreasing alternating field (AF). ARM is qualitatively similar to TRM without the

chemical changes that may be caused due to heating (Banerjee & Mellema 1974). By measuring the specimen's directional dependence for susceptibility or ARM, a second-rank tensor can be determined that mathematically describes the specimen's response to an applied field. This tensor can be used to correct the laboratory TRM measurements and arrive at a more accurate ancient field intensity estimate.

1.3.5 Hysteresis

Hysteresis is the magnetic reaction of a substance under a cycling, induced magnetic field. Hysteresis loops are graphical representations of this reaction and can be used to interpret a number of mineralogical characteristics of the material including the concentration of ferromagnetic material, its average domain state behavior, the relative stability of magnetic grains, anisotropic effects, and paramagnetic or diamagnetic contributions. How easily the magnetization of magnetic grains respond to an external field, by changing their magnetization in the direction of that field, indicates the stability of the magnetic grains and their ability to carry a remanence (Tauxe, 2010).

Paramagnetism is the temporary induced alignment of magnetic moments (in non-ferromagnetic materials) parallel to an applied field. Typical paramagnetic substances include phyllosilicate clays and micas, such as kaolinite and biotite, and iron sulfides and carbonates, such as pyrite and siderite (Moskowitz, 1991). These substances show no net magnetism at room temperature, but display a net magnetization in an applied field because they have unpaired electrons in partially filled orbitals. Their magnetic

susceptibility is strongly temperature dependent (Moskowitz, 1991; Petrovsky, 2007). Diamagnetic materials also have no net magnetic moment in a zero field, but this is because they have no unpaired electrons and their orbital shells are filled. Unlike paramagnetic materials, diamagnetic materials are not temperature dependent and align their magnetic moments antiparallel to an applied field (Moskowitz, 1991; Petrovsky, 2007). Quartz, calcite, and water are typical diamagnetic materials.

Figure 1 outlines a generalized hysteresis loop for a ferromagnetic material and the relevant magnetic parameters that it usually captures. An increasing magnetic field (H) is applied to a specimen and the magnetization (M) of the specimen changes in response. As the applied field increases, the magnetic moments of the grains in the specimen align parallel to the field. At some point the specimen reaches saturation magnetization (Ms). When the applied field is removed, the moments of the grains flip back to their previous direction or into an angle of least resistance. The resulting zero-field remanent magnetization (Mr) is called the saturation remanence and represents the maximum magnetic recording for the material. The field is then increasingly applied in the opposite direction, progressively flipping the grains until a reverse saturation magnetization is reached. The field is reversed again, completing the loop. The saturation magnetization is a direct indicator of the concentration of ferromagnetic material in the sample.

The bulk coercivity (Hc) is the average field strength needed to flip the moment of the grains. The width of the hysteresis loop indicates the average coercivity in a bulk specimen. Wider loops occur in specimens containing a larger proportion of SD grains,

while narrower loops occur in specimens containing PSD and MD grains. Bulk coercivity is a measure of the average stability of the magnetization of the ferromagnetic minerals in the sample. The higher the Hc values, the higher the concentration of stable SD grains are present. Single domain grains are more capable of carrying a remanent magnetization and thus elevated bulk coercivities are viewed as a prerequisite for successful paleointensity experiments.

Specimen magnetizations are also subjected to an increasing reverse field (the backfield curve), which is measured at successive steps in zero field to determine the maximum reverse field required to flip the remanence of single domain grains. This is called the coercivity of remanence (Hcr) and is distinguished from Hc because it is measured with the field off. The smaller the ratio of Hcr to Hc then the more likely the sample is dominated by single domain grains.

Figure 1. Generalized Hysteresis Loop

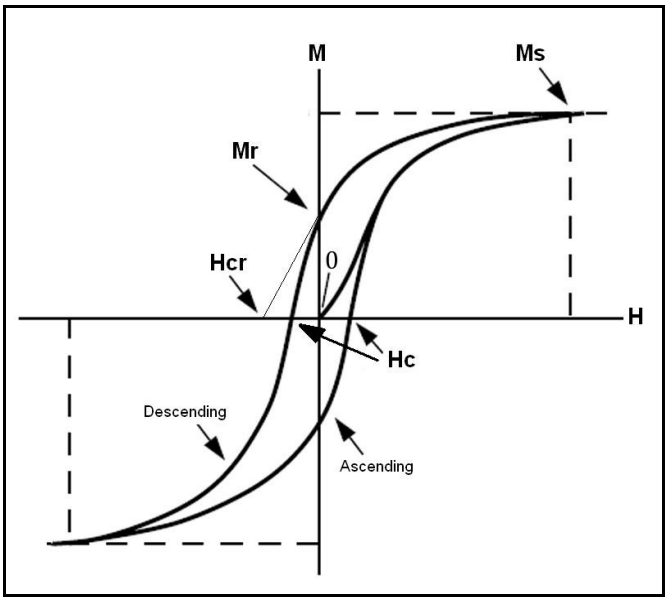

(Adapted from Butler, 1992)

1.4 Paleomagnetism & Archaeomagnetism

Paleomagnetism is the study of the remanent magnetization of the Earth's ancient magnetic field as recorded in volcanic and igneous rocks, soils, and sediments. The subfield of archaeomagnetism involves the study of human-modified materials made of these same substances, such as fired ceramics, brick, and heated rock. Recent research has also found that metal slag, a by-product of iron and copper smelting, also carries a measureable remanent magnetization (Shaar et al., 2010; Ben-Yosef et al., 2008).

Magnetic grains within these materials record the declination, inclination, and intensity of the Earth's field as these materials are originally being formed or deposited. The two most common forms of magnetization in naturally occurring magnetic materials are depositional and thermal remanence (Sternberg, 1990). Depositional magnetization results when magnetic grains in sediments act as tiny compass needles, aligning with the Earth's field as they settle towards a depositional surface. When the sediment becomes lithified the remanent magnetization is locked in place. Materials that formed during exposure to high temperatures record a thermal remanent magnetization (TRM). Heating of archaeological clays to very high temperatures for an extended period resets the original remanence of the constituent materials. Upon cooling, the magnetization of the magnetic particles will become statistically aligned with the Earth's magnetic field at that moment in time.

If archaeological materials undergo heating at temperatures below the Curie temperature of their magnetic particles, the material will record a partial thermal

remanent magnetization (pTRM) or secondary magnetic component. A secondary remanence is one that follows and partially obscures the primary remanence. This can occur due to lightning strikes or other instantaneous magnetizations, called isothermal remanence (IRM); a chemical alteration (CRM), which can occur if hematite precipitates from iron-rich sediments (Dunlop and Özdemir, 1997); and/or prolonged burial with exposure to weak fields, called viscous remanence (VRM) (Pullaiah et al., 1975). Secondary magnetization is often found in pottery due to processes such as successive reheating, as might be found in cooking vessels, or by weathering, such as might occur during saturation of the pottery with water after burial (Yu, 1990). The vector sum of all these magnetic components is called a sample's Natural Remanent Magnetization (NRM).

Archaeomagnetic research frequently examines in-situ heated materials, such as kiln walls or bricks, which can yield both magnetic direction and intensity measurements. Materials found displaced from their original formation context, typically fired pottery that has been removed from the kiln, will yields only intensity measurements. Inclination can occasionally be extracted from displaced ceramics if there is dependable *a priori* knowledge about the original firing position of the object. While the most accurate and complete magnetic analysis would include both directional and intensity data, intensity alone is still useful for quantifying secular variation and compiling reference curves for archaeomagnetic dating. The pottery sherds used in this study were not found in their original firing context; therefore, results are based on intensity measurements alone.

1.5 Applications of Archaeomagnetism

Archaeomagnetism has a number of uses beyond identification of remanent magnetization. It has been used to map the movement of the geomagnetic North Pole for the past 400 years, to investigate geomagnetic dynamo processes, and to observe intensity fluctuations within times of constant polarity. Archaeomagnetic data has also been used to create geomagnetic field evolution models (Butler, 1992), to understand sediment deposition, and to identify unusual geomagnetic "jerks" (rapid directional change) or "spikes" (rapid intensity change), which are often temporally related to episodes of regional and/or global climate change (Gallet, 2006). Magnetic susceptibility of archaeological materials has been used to provenance the geological sources of granite used in Roman column construction and identify metal slag types from iron-smelting sites (Sternberg, 2008). In addition, because the Earth's magnetic field strongly influences the penetration depth of cosmic rays into the upper atmosphere, which has a direct effect on the production of Carbon 14 (^{14}C), archaeomagnetic data is essential for the calibration of radiocarbon dating curves (Sternberg, 1990).

The primary use of archaeomagnetism relevant to this research is the creation of secular variation reference curves that can be used to provide absolute dating curves in archaeological investigations. Archaeomagnetic research has resulted in the development of secular variation curves spanning over 5000 years at sites throughout much of Western Europe and the Americas and nearly 8000 years at sites in Eastern Europe and the Near East (Genevey et al., 2003; Kovacheva, 1997; Sternberg, 2008). These variation curves

are important because they allow researchers to date archaeological materials or sites that are not amenable to dating using traditional archaeological dating methods. For example, archaeomagnetic techniques are well suited to sites that do not contain sufficient uncontaminated organic materials for radiocarbon dating (Leonhardt, 2010; Sternberg, 1990). Alternatively, if archaeological materials at a particular location are considered well-dated, as is the case with the pottery found at Tell Mozan, then archaeomagnetic data acquired from these materials can be leveraged to improve existing secular variation curves for that region.

Section 2. Previous Archaeomagnetic Research

2.1 Addressing Methodological Accuracy

After the initial introduction of archaeomagnetic research (*see section 1.1*), which focused on identifying remanent magnetization, the primary goals of archaeomagnetic research during the second half of the 20th century were the refinement of testing methodology and the narrowing of resulting data scatter. Methodological issues addressed included the determination of original firing position, proper sampling procedures, and testing accuracy. The most accurate archaeomagnetic dating curves include measurement of both magnetic direction and intensity. If ceramics and bricks are not found in-situ within their original firing kiln, for example, directional data cannot be accurately measured and results will be based on magnetic intensity alone. Some of the earliest archaeomagnetic research is now considered unreliable, due to assumptions such as the consistent upright firing of pottery (Aitken and Weaver, 1962), which led some early researchers to assume inclination could be accurately measured on all displaced ceramics. This idea has been disproven with ethnographic studies of pottery manufacture, which show that pottery is not necessarily stacked upright during firing, but can be fired in numerous positions, even in a jumbled pile within the same kiln or firing pit (Rice, 2005). Therefore, unless there is unambiguous evidence for the original firing position of a displaced object, it is best not to attempt to recover inclination.

During the first real surge of archaeomagnetic research in the late 1960s, pioneers in the field such as Aitken, Weaver, and Hawley, focused on testing samples from kiln walls, objects that could be considered in-situ since their last use. Using refined paleomagnetic testing methodology, developed by Thellier and Thellier (1959), they produced a number of secular variation curves and suggested their use as master dating tools in archaeology (Sternberg, 2008; Aitken and Weaver, 1962). The Aitken and Weaver (1962) variation curves relied primarily on declination and inclination data derived from ancient British kilns, and merely noted the importance of intensity as a third component to distinguish between directional measurements that were similar but from obviously different time periods.

In 1966, Weaver conducted progressive heating and cooling intensity experiments on 3rd and 4th century CE archaeological materials using modern samples as controls, with the goal of determining the accuracy of intensity measurements. Basing his experiments on the methods and results of Thellier and Thellier (1959), who estimated that the intensity of Earth's field was slowly decreasing at a rate of approximately 3% per century, Weaver attempted to determine if 3% accuracy in intensity could be achieved. His results, which were closer to 10%, highlighted two important considerations for methodological accuracy: whenever possible, samples should be heated to temperatures above their Curie point, and consistency in measurement procedures must be maintained, such as sample alignment within the testing equipment and accurate temperature controls. In addition, Weaver added pTRM and stability checks to account for secondary magnetization components and possible mineralogical alteration due to heating.

2.2 Narrowing Data Scatter

For the next twenty years, research continued to focus on developing and refining secular variation curves by addressing the issue of data scatter, fluctuations in data points that cause noise or large deviations in curve results. This was achieved by adding more data through additional measurements, utilizing additional curve calibrations and using new statistical modeling techniques. Collection of more archaeomagnetic samples naturally aided in more accurate curve construction and allowed dating curves to be pushed further back in time, well into the Iron Age for most of Europe, to the Bronze Age in Eastern Europe (Genevey et al. 2003; Kovachava, 1997; Rusakov & Zagniy, 1973) and Egypt (Anthavale, 1969; Leonhardt et al., 2010) and even to the Neolithic at Çatal Hoyük in Anatolia (Bucha & Mellaart, 1967). Bucha and Mellaart (1967), for example, tested 7th and 6th millennium BCE archaeological samples from in-situ hearths, oven floors and baked brick, previously dated with radiocarbon dating, to expand on previous curves for the region.

Calibration of archaeomagnetic results is obtained by comparison with traditional archaeological dating techniques, such as stratigraphic sequencing and radiocarbon dating, complementary paleomagnetic data, and/or statistical analysis of data scatter. Archaeomagnetic research in the North American Southwest and Mesoamerica, dominated by DuBois in the 1970s and Eighmy and Sternberg in the 1980s (Eighmy & Sternberg, 1990), produced curves that were calibrated with dendrochronological data, currently the most accurate absolute calibration method (Sternberg, 2008).

Paleomagnetic analysis of Mt. Etna lava flows in Italy was used as an absolute dating complement along with relatively dated archaeological stratigraphy by Tanguy (1970); and Thompson et al. (1974) used paleomagnetic results from stratigraphic sequences of lacustrine lake sediments as a complimentary calibration for their chronological dating of Aechulian sites in Suffolk, England.

In 1970, Burlatskaya et al. addressed the issue of data scatter by attempting to refine inclination and intensity curves for the Ukraine, Caucuses and Moscow by applying a 100 year "moving time window" method (Sternberg, 2008, 985), also called the "moving average" in statistics. Burlatskaya et al. used a weighted moving average over a fixed window of 100 years, and repeated at intervals of 50 years. The moving average statistical method addresses errors in both magnetic directional data and time, and is ideal for curve construction because it reduces short-term fluctuations and highlights long-term trends in time series data (Sternberg and McGuire, 1990a).

2.3 Refining the Methodology

A resurgence in archaeomagnetic research occurred in the late 1990s as methodologies were further refined and access to new technologies and computer controlled equipment narrowed methodological error and significantly reduced the time spent testing samples, from several months to several weeks. Advances allowed researchers time to consider the applications of archaeomagnetism to a variety of new archaeological research questions (Sternberg, 2008). For example, one of the most

important findings was the confirmation that global intensity of the Earth's magnetic field has been gradually decreasing since the first millennium CE, as suggested by Thellier and Thellier in 1959 (Sternberg, 2008). The Thellier stepped heating procedure was further adapted using the IZZI protocol, by Tauxe and Staudigel (2004). The IZZI protocol involves reversing the double heating procedure at every other step so that the sample is heated at the same temperature twice (but not successively), once with an externally applied field (inducing pTRM acquisition) and once at zero field (removing the induced pTRM). The IZZI protocol method allows for the identification of magnetic domain states and mineralogical changes through the use of "tail checks" and pTRM checks, respectively. Because the demagnetization of a SD grain at each temperature step during heating should be independent of the next temperature step, these checks identify if grains are unblocking below their blocking temperature, which may indicate a secondary remanence.

As more archaeomagnetic data were produced, it became apparent that the use of different methodologies could result in different measurement errors. In addition, base curves constructed with the same direction and intensity measurements but using different mathematical modeling could result in variable interpretations of archaeological dates (Lanos, 2005; Sternberg, 2008). New mathematical modeling, such as expansion of the moving window method of Burlatskaya et al. by Sternberg and McGuire (1990b) and Bayesian hierarchical statistics by Lanos (2005), were utilized to construct more accurate dating curves. Lanos, for example, realized that archaeological sites, samples and subsamples (specimens) can all have a number of random and systematic errors

associated with measurement of magnetic direction and intensity. For example, errors associated with displacement of materials in the field, inconsistencies in specimen orientation in the magnetometer, statistical interpretation inaccuracies, incorrect transfer of reference marks from sample to specimen, or heterogeneity of magnetic minerals within specimens. In addition, there is error associated with comparing time periods between sites and the number of data points represented in the moving window technique. Different window "widths", from 25 to 100 years, and even combinations of windows (Sternberg and McGuire, 1990b), have been used to construct archaeomagnetic curves, and variability in number of sites or samples represented in each window introduces another level of error into the final results. Comparison between traditional, stratified statistical models and Bayesian hierarchical models by Lanos, performed on previously published data, found that the hierarchical models correct for curve distortions resulting from the preference of moving window averages to favor samples with greater specimen numbers and sites with greater sample numbers (Lanos, 2005). Lanos found that curve precision is related to the number and precision of data points within the moving window, and emphasized the need for more data measurements per site.

A number of reference curves have been produced and are continually being refined for specific regions as more archaeological materials are analyzed. Lodge and Holme (2008), for example, derived a new European reference curve model, called GMADE2K.1, covering the last 2000 years. New web interfaces for archaeomagnetic databases, such as GEOMAGIA50, hosted by Scripps Institution of Oceanography at University of California, San Diego, allow for interactive access and curve construction

using archaeomagnetic data uploaded from around the world. The GEOMAGIA50 database contains nearly 8000 field results spanning the past 50,000 years and allows for selection of individual parameters, such as modeling statistics, geographic and age constraints, and magnetic testing methodology (GEOMAGIA50, 2011). In addition, GEOMAGIA50 generates a number of global geomagnetic models, three of which can be used as generalized archaeomagnetic curves: ARCH3K.1, CALS10K.1b, and CALS3K.4. The ARCH3K.1 model consists of archaeomagnetic data biased towards the northern hemisphere, while the CALS3K.4 is generated by combining archaeomagnetic and lake sediment data. Both use data covering the last 3000 years (Donadini et al., 2006; Korhonen et al., 2008). The CALS10K.1b model covers the past 10,000 years and utilizes both archaeomagnetic and lake sediment data. This model uses bootstrap sampling to account for uncertainties and is, therefore, strongly smoothed (Korte et al., 2011). Figure 2 displays a typical curve generated in GEOMAGIA50 using each of the three models. The models highlight the data points from four different studies conducted on archaeological bricks, pottery and other ceramics in Syria. All but one data point come from three of the four studies discussed below in Section 2.4. While these global geomagnetic models capture broad trends in the behavior of the Earth's magnetic field, they are of limited use in archaeomagnetic dating because of the smoothing that is inherent in their construction. The final archaeointensity curves used in this study will be generated using statistical modeling in Mathmatica and focus on the period between 3000 BCE and 0 CE.

Figure 2. Magnetic Intensity for Syria

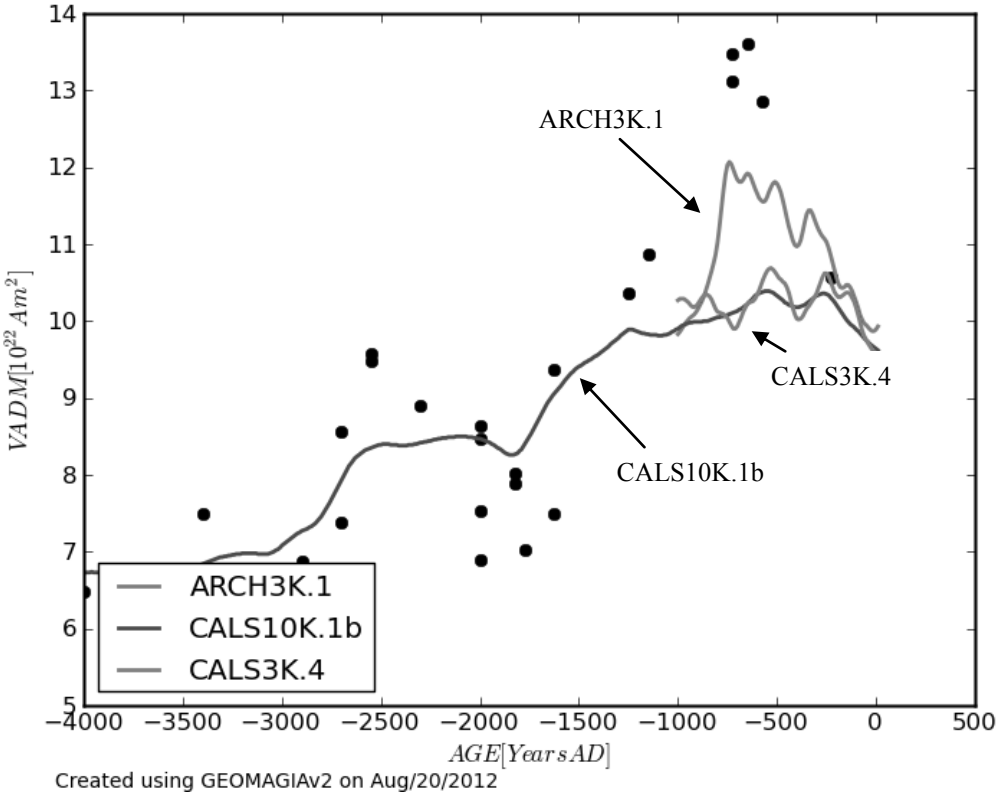

(Donadini et al., 2006; Korhonen et al., 2008)

2.4 Previous Research in Syria

Archaeomagnetic research in Syria has been dominated by French researchers Gallet, Genevey, Le Goff, and Margueron, who have acquired magnetic field results from over a dozen archaeological sites in the country spanning nearly eight millennia (Gallet et al., 2008; Gallet et al., 2006; Gallet and Le Goff, 2006; Genevey et al., 2003). In 2003, Genevey et al. presented archaeomagnetic results on twenty groups of pottery sherds and brick fragments from eleven different sites, all of which were considered well-dated

using ceramic typology, diagnostic artifacts such as cylinder seals and inscribed clay tablets, and/or stratigraphic context. Each group consisted of six to eight samples selected based on their locational context. To reduce the effects of anisotropy and data scatter due to secondary magnetization, the authors only selected objects with a fine clay matrix (few large inclusions), a thick wall (in the case of pottery), and no indication of re-firing. In addition, preliminary low-field susceptibility tests were conducted up to a temperature of 550°C to check for reversibility of heating and cooling curves. Their magnetic mineralogical results indicated that samples were relatively homogenous despite manufacture date or process. Hysteresis measurements and thermomagnetic curves indicated that all samples most likely contained titanomagnetite in the PSD range.

The primary thermal demagnetization method used in the above studies was a modification of the Thellier and Thellier (1959) method by Coe et al. (1967), which performs the zero-field step prior to the in-field step during heating. Anisotropy of TRM was determined in order to correct raw intensity data and the cooling rate effect was measured to determine the accuracy of TRM acquisition. Each specimen was tested at three cooling intervals: five, ten, and thirty hours. The mean correction factor of intensity for the cooling rate effect was found to be similar for all three intervals. Final intensity results indicated a somewhat steady field intensity value ranging from 30 to 40 μT between 6000 and 3500 BCE and a significant field intensity increase between 3500 and 700 BCE. During the latter interval, a moderate decrease occurred between 2550 and 1750 BCE followed by a relatively abrupt rebound resulting in a spike in intensity around 700 BCE. Results were compared to intensity curves from Egypt, Greece and Georgia,

obtained by different researchers using similar methodologies, which showed acceptable agreement between curves for the eastern Mediterranean region for the last four millennia and no indication of major longitudinal intensity drift caused by non-dipole features for the region (Genevey et al., 2003). This suggested a larger, regional archaeointensity curve, spanning from Greece to Georgia, a distance of approximately 2200 km, was suitable as a base curve having a low error rate.

In 2006, Gallet and Le Goff developed an automated procedure for high-temperature testing of samples in as little as two hours. A three-axis or triaxial vibrating sample magnetometer (Triaxe) allows for in-field magnetization measurements and corrections for TRM anisotropy and the cooling rate effect within one piece of equipment. Results from eighty pottery sherds and baked brick objects from five different archaeological sites, several of which had been previously tested using the Thellier and Thellier (1959) Coe (1967) method, confirmed the rapid intensity increase between 2000 and 750 BCE found in previous research and provided additional refinement of the curve for the last 4000 years. In addition, the occurrence of an additional intensity spike around 2800-2600 BCE was identified. In a separate study (Gallet et al., 2006), magnetic intensity measurements were conducted on baked brick from archaeological sites in Syria and Iran using both the Triaxe and Thellier and Thellier (1959) methods, resulting in thirty-one new mean intensity values. These results identified four archaeomagnetic spikes occurring between 2800-2600 BCE, 2100-1900 BCE, 1750-1500 BCE, and at 750 BCE.

Additional study with the Triaxe method was carried out at four archaeological sites representing archaeological dates between 2500 and 1600 BCE (Gallet et al., 2008). Results were in agreement with previous intensity results obtained by the authors at the same sites, further refining the intensity curve and again highlighting the occurrence of three archaeomagnetic spikes for the region, at 2600 BCE, 2300 BCE and 1600BCE. Some of these abrupt increases in the intensity appear to coincide with climatic cooling events recorded in deep sea sediment cores in the North Atlantic and lacustrine cores from Sweden (Gallet et al., 2006). These cooling events appeared to be temporally associated with episodes of social change and political instability in the Near East, leading the authors to suggest a link between geomagnetic field behavior and human history during the first three millennia BCE in Mesopotamia. Despite the temporal association of these observations, more research is required in order to better understand any relationship between the strength of the geomagnetic field and global climate.

Section 3. Site Description

Tell Mozan, identified as the ancient city-state of Urkesh, was the political and religious center of the Hurrians, a distinctive culture with a unique language that inhabited the Syro-Mesopotamian region during the 4th and 3rd millennia BCE (Buccellati, 2007; 2005). Mozan is located near the interface between the Taurus Mountains of Anatolia and the Mesopotamian lowlands, in the Syrian piedmont region located along the northern edge of the area traditionally known as the Fertile Crescent (37°03'24"N, 40°59'45"E, elev. 463 m). The Tell rises from the agricultural plain near one of the seasonal wadis that flow into the Khabur River, a major tributary of the Euphrates (Figure 3). Historically, the Hurrian culture was considered a small vassal of the Akkadian empire (circa 2300-2200 BCE). However, Urkesh's strategic geographic location not only benefited from the fertile agricultural plain but enabled the Hurrians to control trade in copper and other mineral deposits coming down from the Anatolian highlands (Buccellati, 2005). This mountainous backdrop also helped the Hurrians maintain a unique ethnic and religious identity, buffering them from the expanding Akkadian and Sumerian empires to the east and south (Buccellati and Kelly-Buccellati, 2005).

Figure 3. Location of Tell Mozan, Syria

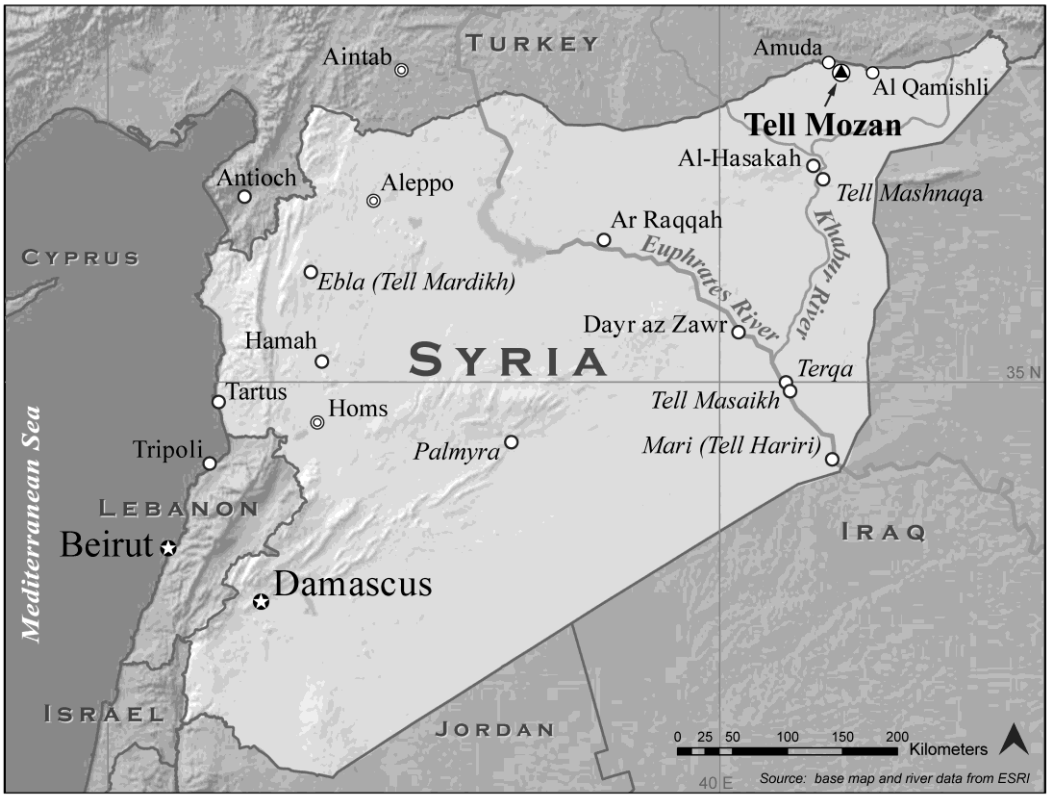

Excavations at Tell Mozan have uncovered numerous cuneiform tablets and over 100 different seals with textual inscriptions, including seals belonging to the royal household containing uniquely Hurrian nomenclature. Seals belonging to Tar'am-Agade, daughter of the Akkadian king Naram-Sin, indicate that she was most likely a queen at Urkesh, further evidence that Urkesh remained an independently ruled political and religious urban center (Buccellati, 2005). The entire site covers nearly 16,000 square meters and is dominated by several major architectural features including an Early Dynastic temple complex (circa 2800 to 2300 BCE), a large royal palace structure

constructed during Tupkish's reign (2269-2240 BCE), a number of courtyards and private houses associated with the palace, and an impressive, ceremonial pit-like structure located near the palace, which is interpreted to be a ritual *âbi* constructed in the late 3rd to early 4th millennium BCE.

There are six primary occupational phases of Urkesh investigated in this study. Table 1 outlines the general chronology of the site by stratigraphic phase as defined by Buccellati (2003) including a description of the settlement patterns for each phase, the associated reigning period of Urkesh as determined from archeological and textual evidence, and the site chronology as it relates to other archaeological periods previously defined for Mesopotamia and Syria. Pottery sherds used in this archaeomagnetic research were collected from units A9, A14, and A16 and are associated with phases 1 through 7 of the Royal Palace complex at the site (Figure 4). Phases 1 through 6 constitute the primary occupations levels and yielded the most significant pottery samples. Phase 7 is associated with a highly disturbed stratigraphic layer at the surface affected by severe erosion and recent use by nomadic populations. Phase 7 pottery sherds are presumed to range from the post Mitanni period to the present day, however, the degree of erosion at the surface has also exposed materials from earlier time periods. Therefore, the exact chronological association of phase 7 samples is unknown. Results from archaeomagnetic measurements will be used as a guide for archaeointensity dating of the phase 7 samples and sample 35 which did not have an associated phase date. Phase 2 palace samples were unavailable at the time of this study.

Table 1. General Chronology of Urkesh and Associated Archaeological Periods

(Adapted from Buccellati, 2003)

Site Phase	Description	Urkesh	Syrian	Mesopotamian
7	no known occupation at site	Ancient to modern	Ancient to modern	Ancient to modern
6	scattered occupations		Mittani	Middle Babylonian/Kassite/Hittite (1595-1200 BCE)
5	last settlements beginning with expansion over scattered occupations and ending in collapse	Terru, Haziran	OJ II to OJ III	Old Babylonian-Khabur (1900-1595 BCE)
4b	middle settlement north, scattered occupation south		OJ I	Isin-Larsa (2000-1900 BCE)
4a	lower settlement north, scattered occupation south	Ann-atal, Atal-šen, Sadar-mat	EJ V	Ur III (2112-2004 BCE)
3b	palace dependency, continued re-use		EJ IV	Post-imperial Akkadian (2192-2112 BCE)
3a	palace dependency, destruction and first re-use under Tar'am-Agade	Tar'am-Agade		Naram-Sin/Šar-kali-šarri (2240-2193 BCE)
2	Palace construction and occupation of Tupkish Palace	Tupkish	EJ III b	Man-ištu-šu/Naram-Sin (2269-2240 BCE)
1	Pre-palace, continued use of ābi	Tiš-atal		Sargon/Rimuš (2334-2270 BCE)
NA	Temple complex and external city walls constructed		EJ III a	Early Dynastic III (2500-2334 BCE)
NA	Construction and first use of the ābi, construction of inner city wall, terracing below temple complex	Urban beginnings		Early Dynastic II (2800-2500 BCE)

Figure 4. Plan of Royal Palace Area A

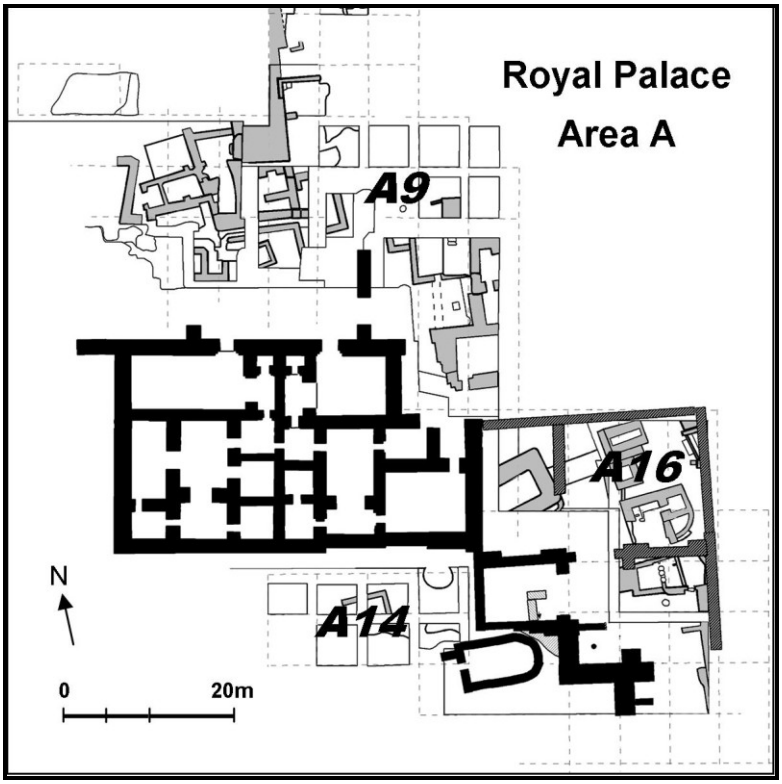

(*Adapted from Frahm, 2010*)

Section 4. Methods

4.1 Sample selection and preparation

To obtain the best representation of the chronology at Tell Mozan, ninety-five different pottery sherds from archaeological phases 1 through 7 were briefly surveyed for archaeomagnetic testing suitability. Sample sherds were selected based on their degree of firing, the porosity of their clay matrix, amount of temper, and suitable size (See Appendix A, Table A1 for full sampling criteria results). Table 2 briefly outlines each sample chosen, its associated phase, degree of firing, color, and ware type. Degree of firing was the most important selection criteria, as the remanent magnetization held by the pottery sherds was thermal in origin. Samples were chosen to ensure that the pottery had been fully fired to high temperatures, presumably above the Curie temperature of their magnetic components. Firing in an oxygen-rich kiln at high temperatures (above 600°C) for a sufficient length of time leads to full combustion of organic material in the clay and a bright orange to red coloration of the final ceramic. These types of conditions are considered oxidized. Reduced conditions, those lacking sufficient oxygen, can result in incomplete combustion of organic material and a final ceramic that is grey in color. Reduced conditions are often associated with low temperature or incomplete firing time (Rice, 2005). Samples that appeared fully oxidized had a homogenous color throughout and ranged from light buff/beige to dark red in color, indicating variable iron concentrations (Figure 5). Samples that were incompletely fired, as evidenced by organic

inclusions or a dark unoxidized core (a sandwiched oxidized/unoxidized/oxidized cross-section) were rejected. Organic inclusions are not fully removed until temperatures in the kiln reach 750°C (Rice, 2005). The necessary Curie temperature for resetting magnetization of magnetite grains is 580°C. The exception to this selection criterion was sample 40 from phase 1. This sample appeared fully oxidized prior to cutting but subsequently displayed a very faint grey, possibly unoxidized core. As suitable samples for phase 1 were lacking, it was included in this study.

Ceramic ware types, as defined by Marilyn Kelly-Buccellati (Urkesh Global Record), are primarily based on clay temper. Mozan ware types are classified as Chaff (CH), Fine Chaff (FC), Red-Orange Calcite (RC), Sand (S), or Imitation Metal (IM). These wares contain various proportions of chaff, calcite and sand temper, the majority component defining the ware type. Imitation Metal wares are an indication of color more than temper as these samples are grey. They will be referred to as grey wares from here on. By the end of the 2nd millennium BCE and into the Iron Age, grey ware pottery became popular, with highly burnished pieces presumably imitating containers made of metal (Dyson, 1968). Sample 58 was unique in decoration, highly burnished with a dark red slip or glaze, and classified as a Burnt Red ware (BR). According to the Urkesh Global Record, Chaff and Fine Chaff ware types were believed to be fired at medium temperatures and Red-Orange Calcite wares were believed to be fired at medium to high temperatures, however, an estimate of these firing temperatures was not given in the database. Most samples appear to be typical earthenware pottery, which is fired to temperatures between 900°C and 1200°C, although some may be high-fired terra-cottas,

which are ceramics fired below 900°C.

Table 2. Tell Mozan Pottery Samples

Sample ID	Site Phase	Archaeological Date (BCE)	Degree of Firing	Color	Ware Type
Unit A9					
9	6	1595-1200	O	Buff	FC
13	5	1900-1595	O	Red	FC
14	5	1900-1595	O	Orange	FC
23	6	1595-1200	O	Orange	RC
Unit A14					
32	4	2112-1900	O	Orange[2]	RC
35	*	*	O	Buff	FC
37	*	*	R	Grey	IM
40	1	2334-2270	R[1]	Greenish Buff	S
51	4b	2000-1900	O	Orange	RC
54	7	1200-modern	R	Grey	IM
56	1	2334-2270	O	Greenish Buff	S
58	7	1200-modern	O	Red[3]	BR
64	3	2240-2112	O	Buff	FC
65	3	2240-2112	O	Buff	FC
72	4	2112-1900	O	Red	RC
Unit A16					
mdS01	3b/4	2192-2004	O	Orange	FC
mdS04	3b/4	2192-2004	O	Buff	FC

Pottery samples chosen for testing were either fully oxidized (O) or reduced (R) but high fired. Ware Types: FC = Fine Chaff, RC = Red-Orange Calcite, IM = Imitation Metal, S = Sand, BR = Burnt Red Ware.

** Samples 37had no associated phase data and therefore, no known date, sample 35 was dated to phase 3 after testing began.*

[1] Sample 40 had a faint carbon core

[2] Sample 32 had an orange exterior, red interior

[3] Sample 58 had a red exterior, orange interior

Samples were also selected to have a fine clay matrix or texture and no large inclusions, to ensure that the grains carrying magnetic remanence were similar in size. Samples with large pore spaces were excluded to ensure structural stability during thermal experiments, as highly porous materials can fracture during successive heating. Additionally, two samples of dark grey ware (IM) pottery were included to verify their suitability as archaeomagnetic samples. These samples, 37 and 54, were extremely fine textured and stoneware-like in hardness. Firing temperatures of 1200°C to 1350°C are necessary to produce stonewares (Rice, 2005). By the Bronze Age in the Near East, kiln firing was well developed and could have feasibly reached these high temperatures. As both of these samples are typical of grey ware pieces from the Iron Age or later, they may have been from kilns fired in a high enough heat to remove organic material but in a reducing environment. Finally, samples were selected to represent each occupational phase. Most samples were typical of Bronze Age household pottery for Syria with the exception of Phase 1 samples (40 and 56). These samples where characterized by a green to greenish beige color and had an extremely fine texture. These samples represent typical Syrian palace wares that were finely levigated during clay production. A minimum of two samples from each phase were chosen. Samples 35 and 37 had no known phase data recorded in the Urkesh Global Record. Sample 37 is typical of Iron Age and later period grey wares and most likely originates from phase 7, a highly disturbed layer which contains artifacts from multiple time periods. Sample 35 is another finely levigated, very light buff ware that looks similar to pottery from phases 3 and 4.

These samples were included in this study in anticipation that their possible age could be identified after final analysis.

Figure 5. Representative Samples

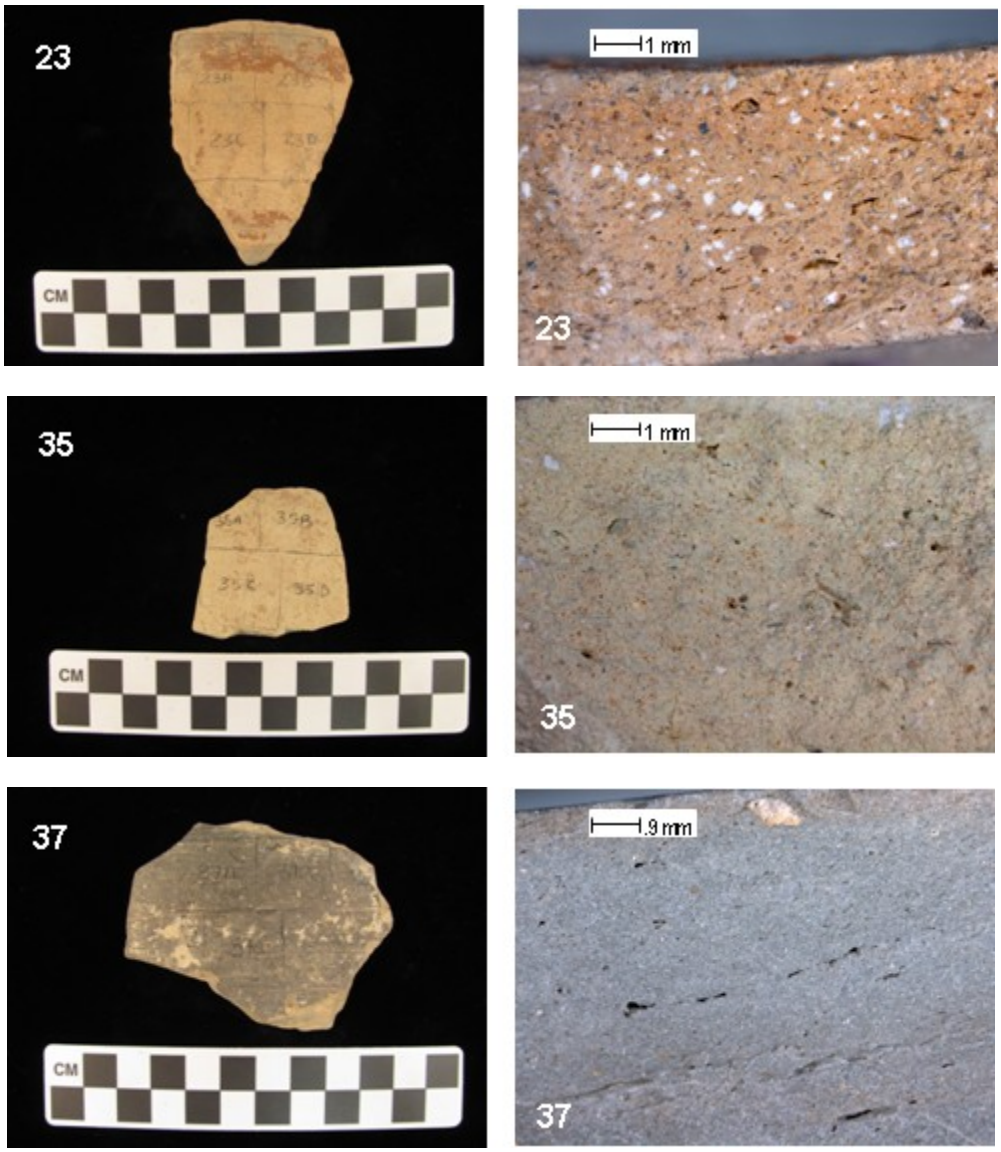

Of the ninety-five sherds obtained from the site, thirty-four were suitable samples for magnetic study; however, only seventeen were of suitable size for subdivision into four 2 cm x 2 cm replicate specimens (Figure 6). Each sample was photographed after marking to record the orientation and relationship of each specimen prior to cutting. Cross sections of each sample were photographed using the Leica MZ16A Microscope and can be found in Appendix A. Specimens were cut using a Stuers Discoplan TS saw and the exterior and interior surface of each specimen was distinguished by a bevel of 45° cut into the NE corner to aid in orienting all specimens the same while testing. In all experiments, samples were oriented so that the Z axis was parallel to the plane of the sample.

Most samples were relatively clean of debris; however, samples 37, 40, 54, 58, and 72 had a large amount of hard secondary calcite accumulation on the interior surface (40, 58, and 72), exterior (54), or both (37). Sample mds04 had a thin black layer poorly applied to the interior, which could have been paint or dye stored in the vessel. It did not appear to be from cooking. Sample 40 had a light reddish brown interior stain which did appear to be transferred from the contents stored in the vessel. No specimen appeared to have been used for cooking purposes. Each specimen was sanded using coarse 60-grit silicon carbide sandpaper to remove paint and debris, and then fine-sanded with 320-grit sandpaper. Specimens were then cleaned in double deionized water using a Narda Ultrasonic Cleaner for one minute and then rinsed again in fresh double deionized water. When completely dry, all specimens were weighed on a Sartorius electronic scale and volume measurements were taken with a digital caliper.

Figure 6. Representative Specimen Set

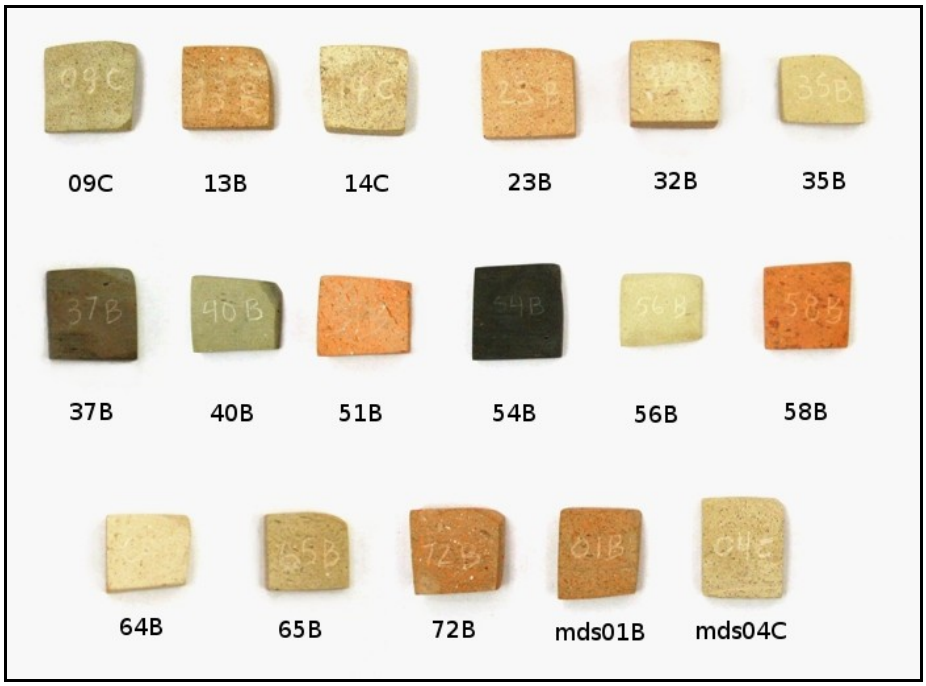

4.2 Magnetic Measurements

4.2.1 Susceptibility and Superparamagnetism

All archaeomagnetic experiments were conducted on equipment at the Institute for Rock Magnetism at the University of Minnesota. Prior to any thermal experiments, a number of ambient temperature experiments were conducted to analyze the suitability of the samples for thermal demagnetization. Low field magnetic susceptibility was measured at room temperature using a Kappabridge KL4-2 Magnetic Susceptibility Meter in a field of 300 A/m and a frequency of 920 Hz with a sensitivity of 4×10^{-8} SI. This was conducted on all specimens to verify internal magnetic homogeneity of the

pottery samples. Susceptibility measurements were repeated four times on each specimen to determine the average susceptibility and the standard deviation around the mean.

Specimen set #1 (containing one specimen from each sample) was tested for the presence of superparamagnetic grains with a Magnon Variable Frequency Susceptibility Meter in a field of 300 A/m. Superparamagnetic grains are so small that their magnetic direction is constantly fluctuating even at room temperature. They will only respond to very high frequency fields, making them unsuitable for archaeomagnetic testing because they do not carry a remanence. In order to determine the percentage of superparamagnetic grains in each sample, one specimen from each sample was subjected to both a low frequency (465 Hz), which affects all grains, and a high frequency (4650 Hz), which should affect a population of smaller grains. Measurements were repeated five times, averaged and the frequency dependency of susceptibility (χ_{fd}) (the percentage of superparamagnetic grains in the specimen) was calculated as:

$\chi_{fd} = 100 \times ((\chi_{low}-\chi_{high})/\chi_{low})$.

4.2.2 Hysteresis

Hysteresis loops and backfield curves at room temperature were generated for specimen set #1 using a Princeton Applied Research Vibrating Sample Magnetometer (VSM) with a sensitivity of 2×10^{-8} Am^2. The VSM applies an increasing external magnetic field from 0 to 1 Tesla (T) and measures the response of magnetic minerals to

the applied field. Hysteresis diagrams and parameters were calculated using in-house software developed at the Institute for Rock Magnetism. See section 1.3.5 for explanation of the measurements generated in hysteresis experiments and their significance.

4.2.3 Alternating Field (AF) Demagnetization

Pottery samples ideally suited for archaeomagnetic measurements will have only one strong component of remanent magnetization. Specimens containing secondary components, if present, are considered acceptable only if the secondary component is weak and removed quickly during alternating field (AF) or thermal demagnetization. Specimen set #1 was AF demagnetized in successive steps from 2.5 to 170 mT using a 2G Enterprises 755 Long Core Magnetometer (referred to hereafter as ”2G”). AF demagnetization effectively “cleans” the sample by applying a sinusoidal magnetic field, which randomizes all magnetic grains with coercivities lower than the peak applied field. The 2G was additionally used to measure initial NRM. The primary magnetization component of interest is the magnetization acquired from firing of the pottery. The results of AF demagnetization are used to determine the stability of the magnetization held by the samples and to identify which samples have single or multiple components of magnetization. Data obtained from AF demagnetization will be used to calculate the median destructive field (MDF), a measure of how strong a field is required to remove half of the NRM. Samples with elevated MDF values are more likely to contain a larger

fraction of single domain grains and are therefore more likely to yield successful paleointensity estimates.

4.2.4 AF Demagnetization of 1Tesla IRM

The ratio of a sample's NRM to its saturation remanence is frequently used as a coarse estimation of the intensity of a sample's original magnetizing field. This method of using the ratio of equivalent magnetizations (REM) to estimate paleointensity has recently been expanded to compare the AF demagnetization spectra of the NRM to that of a laboratory applied 1 Tesla (T) induced remanence (IRM). This REM method was performed on eight of the specimens from set #1 to obtain a quick estimate of their archaeointensity. All specimens were given a maximum IRM of 1T along the Z-axis using a 2G Enterprises IRM Pulse Magnetizer. Specimens were then AF demagnetized along the X, Y, and Z axes in 16 steps, ranging from 2.5 to 170 mT. The remanent magnetization of the IRM was measured on a Schoenstedt Spinner Magnetometer after each step due to the high remanence carried by the specimens. Due to time constraints, the remaining 12 specimens were not measured and the IRM results for the 8 specimens are not considered in the final results.

4.2.5 Remanence Anisotropy

Before remanence anisotropy experiments were run, all specimens from set #1 were demagnetized at room temperature along their X, Y & Z axes using the 1.1 T AF demagnetization function on the Princeton Measurements Micromag Vibrating Sample Magnetometer (with vibration turned off) to ensure the removal of the 1T IRM previously acquired. Samples were further AF demagnetized along all axes in a 200 mT field using a Precision Instruments D-2000 DTECH AF Demagnetizer. These demagnetization routines allow each sample to acquire ARMs from the same demagnetization "starting point". Each specimen's demagnetized state was measured using a 2G RF SQUID Superconducting Rock Magnetometer (SRM). The specimens were then given a 30 μT DC ARM using a 150 mT AF demagnetization field on the DTECH. The ARM was measured on the SRM and the demagnetization/remagnetization procedure was repeated for all six axes.

4.2.6 Thermal Remanent Demagnetization

Archaeointensity measurements were performed on specimen set #2. These specimens had only been tested for susceptibility and initial NRM and were, therefore, completely unaltered from a magnetic perspective. Thermal remanent demagnetization experiments were conducted in a specially shielded room at the Institute for Rock Magnetism where background fields are less than 100 nT. Demagnetization spectra were

acquired using the Thellier-style, IZZI protocol of Tauxe and Staudigel (2004). Samples were heated in air in an ASC Model TD-48SC Thermal Demagnetizer Furnace from a minimum 100°C to a maximum of 600°C. Soak time was twenty minutes and then specimens were cooled to room temperature. In-field steps were performed at 30μT and the laboratory field was applied parallel to the Z axis of the specimens. Remanent magnetization was measured after each heating cycle with the 2G.

Section 5. Results

The results of susceptibility, hysteresis and AF demagnetization experiments were used to characterize the samples and determine their suitability for Thellier-style paleointensity experiments. The results of thermal demagnetization experiments were used in final paleointensity analysis.

5.1 Susceptibility and Superparamagnetism

Susceptibility measurements were collected from three specimens of each sample. Average susceptibility (χ) results for each specimen show that all three specimens from each pottery sample have similar χ values with negligible standard deviations, indicating homogeneously distributed concentrations of magnetic material. In this light, further tests on one specimen can be assumed to be representative of the sample as a whole. Low field (χ_{lf}) and high field (χ_{hf}) superparamagnetic results indicate a low percentage of superparamagnetic grains (χ_{fd}), less than 12% for all specimens. Susceptibility and superparamagnetic results are summarized in Table 3 below and Appendix B, Table B1.

Table 3. Susceptibility Results

Sample ID	Average χ [1] (m^3/kg)	χ_{lf} (m^3/kg)	χ_{hf} (m^3/kg)	χ_{fd} (%)
40	2.26E-07	2.11E-07	2.08E-07	1.63
56	4.18E-07	4.07E-07	3.97E-07	2.30
37	8.53E-07	9.97E-07	9.44E-07	5.31
51	1.95E-06	2.16E-06	1.90E-06	11.97
54	2.01E-06	1.87E-06	1.85E-06	1.08
mds04	2.48E-06	2.42E-06	2.25E-06	6.80
09	3.50E-06	2.92E-06	2.80E-06	3.93
35	3.65E-06	3.70E-06	3.55E-06	4.02
14	3.99E-06	4.05E-06	3.71E-06	8.39
65	4.11E-06	4.13E-06	3.86E-06	6.54
13	4.31E-06	4.15E-06	3.74E-06	9.98
58	4.37E-06	4.49E-06	4.05E-06	9.86
23	4.86E-06	4.96E-06	4.50E-06	9.13
32	5.47E-06	5.75E-06	5.19E-06	9.81
64	5.65E-06	5.54E-06	5.22E-06	5.81
mds01	6.11E-06	6.08E-06	5.46E-06	10.22
72	6.45E-06	6.79E-06	6.13E-06	9.68

1. Susceptibility (χ) is average for all three specimens in the sample.

5.2 Hysteresis & Domain Structure

A summary of hysteresis measurements for each sample is given in Table 4. Coercivity (Hc) values range from 3.7 mT for sample 51 to 25.4 mT sample 54. Coercivity of Remanence (Hcr) ranges from 11.8 mT for sample 64 to 44.8 mT for sample 54. Increasing Hc and Hcr do not seem to correspond with pottery age or ware type. Saturation Magnetization (Ms), on the other hand, indicates that similarly dated pottery samples have similar Ms values. For example, samples 40 and 56, palace type

pottery from phase 1, had similarly low Ms, but sample 56 had more than twice the Hc, 7.8 mT and 16.1 mT respectively. The similar Ms indicates a similar concentration of magnetic minerals, which suggests that the unusual greenish clay for palace wares originated from the same source. The different coercivity may indicate that each piece was made at a different time or by different potters, one being more finely levigated than the other resulting in smaller magnetic grain sizes. Samples 9 and 23 from phase 6 and samples 72 and 32 from phase 4 also showed similar Ms and largely different Hc.

Table 4. Hysteresis Results

Sample ID	Phase	Archaeological Date (BCE)	Ms (Am^2/kg)	Mr (Am^2/kg)	Hc (mT)	Hcr (mT)
40	1	2334-2270	1.39E-02	3.17E-03	7.8	22.1
56	1	2334-2270	1.42E-02	5.33E-03	16.1	28.7
51	4b	2000-1900	3.83E-02	4.44E-03	3.7	15.2
37	*	*	5.53E-02	1.14E-02	14.2	32.0
mds04	3b/4	2192-2004	8.26E-02	2.68E-02	13.6	33.2
65	3	2240-2112	1.10E-01	3.25E-02	7.9	16.1
58	7	1200-modern	1.34E-01	2.38E-02	6.6	15.9
13	5	1900-1595	1.38E-01	2.66E-02	8.3	21.1
14	5	1900-1595	1.48E-01	4.51E-02	12.0	28.5
09	6	1595-1200	1.56E-01	5.69E-02	17.6	32.3
23	6	1595-1200	1.57E-01	3.01E-02	7.4	16.5
64	3	2240-2112	1.67E-01	4.55E-02	6.6	11.8
mds01	3b/4	2192-2004	1.84E-01	3.52E-02	7.2	19.1
54	7	1200-modern	1.95E-01	6.22E-02	25.4	44.8
72	4	2112-1900	2.18E-01	2.51E-02	4.4	14.4
32	4	2112-1900	2.59E-01	7.48E-02	11.6	29.5
35	*	*	4.33E-01	1.12E-01	6.6	12.9

** Samples 37 and 35 had no associated phase data and therefore, no known date.*

All samples displayed a combination of paramagnetic and ferromagnetic behavior in hysteresis measurements and the difference in Ms, Hc, and Hcr across samples was one order of magnitude or less. Figure 7 depicts hysteresis loops for specimens 09b, 23c and 37c, which are representative of all samples. No samples displayed "wasp-waisted" behavior, which occurs when there are two discrete sizes or types of magnetic minerals in the sample.

Figure 7. Representative Hysteresis Loops

Figure 7a. Specimen 09b

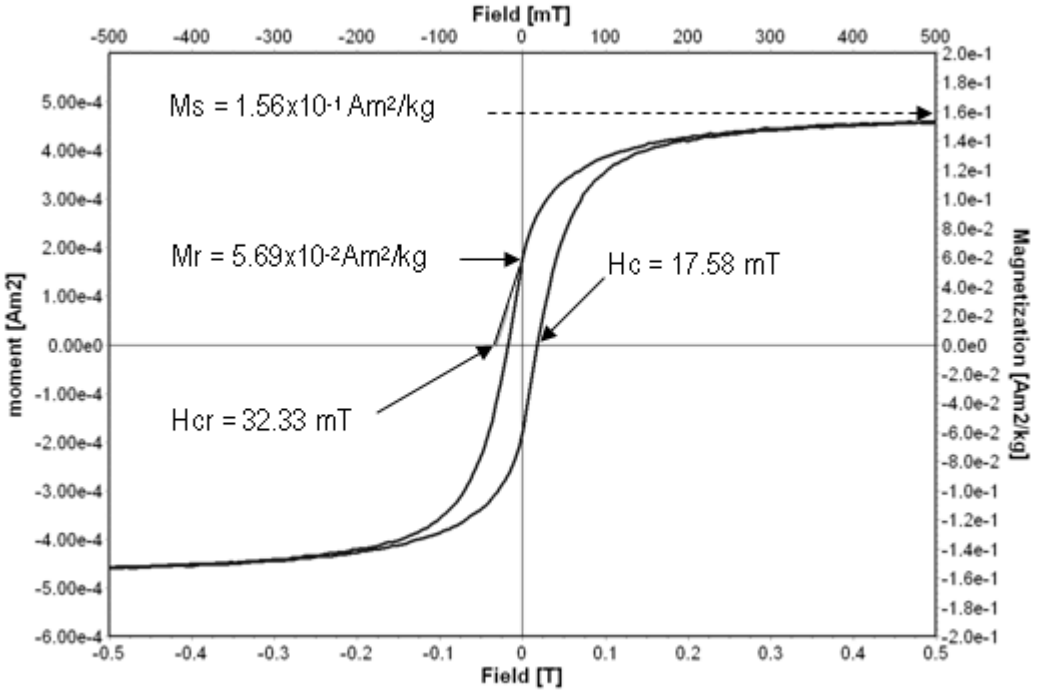

Figure 7b. Specimen 23c

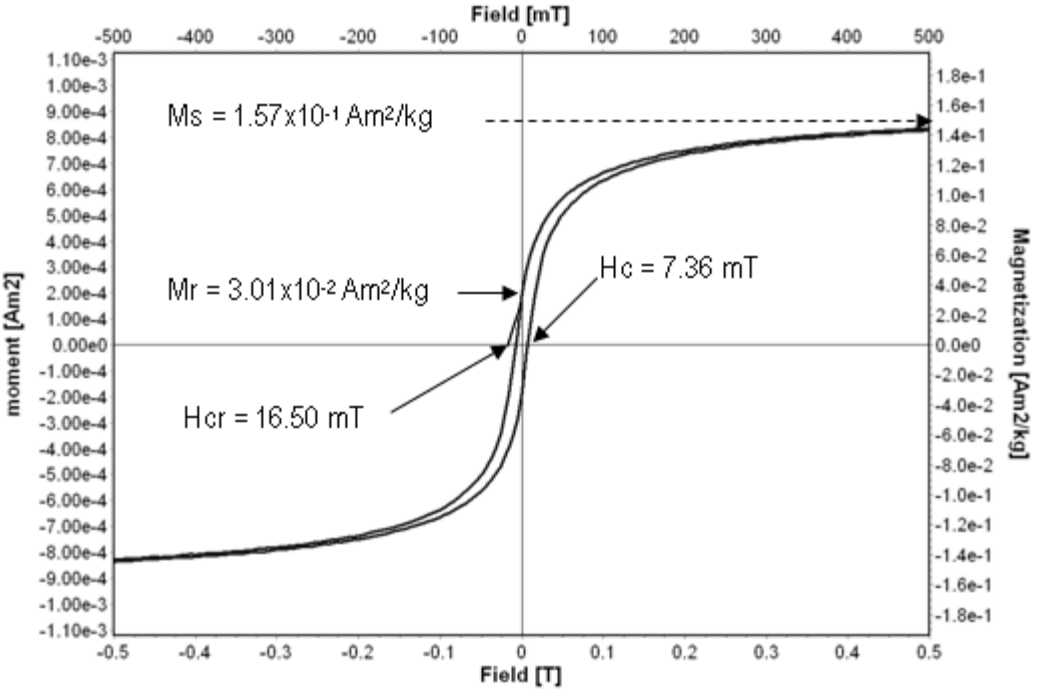

Figure 7c. Specimen 37c

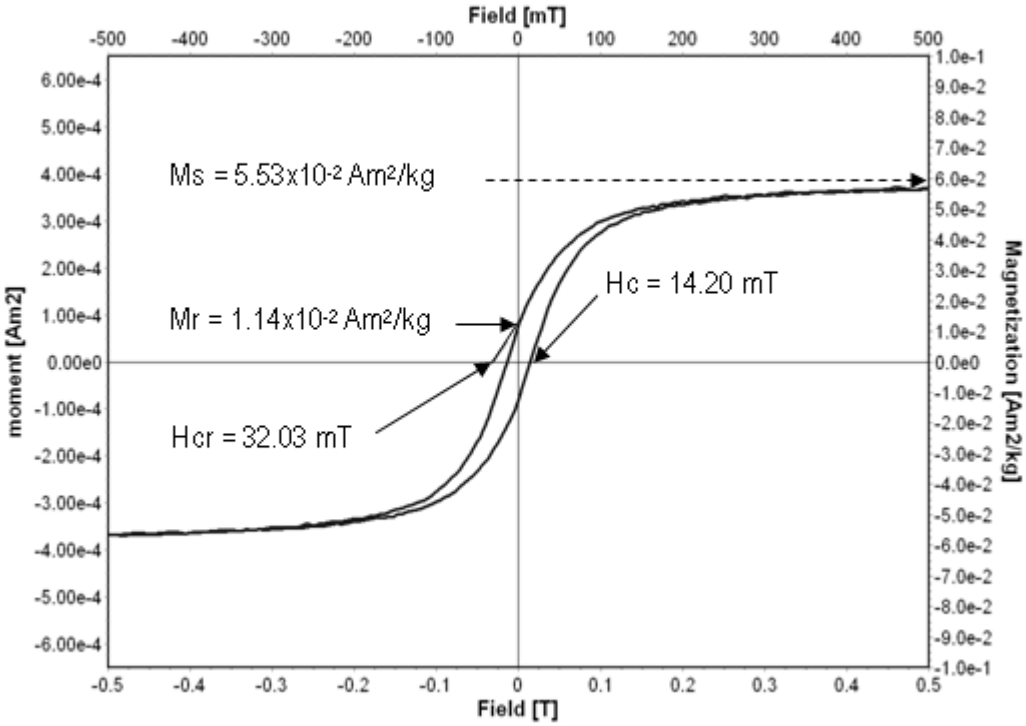

The ratio of the remanent magnetization (Mr) to saturation magnetization (Ms) is called the "remanence ratio." The ratio of the coercivity of remanence (Hcr) to coercivity (Hc) is called the "coercivity ratio." These parameters are frequently used to discriminate the average magnetic domain structure of each sample on a Day Plot (Day et al., 1977) as shown in Figure 8. Ideal samples for paleointensity experiments consist of all SD grains; however, this state is rare. Figure 8 indicates that most samples in this study fall in the PSD range and are likely to contain a mixture of SD, PSD, and MD grains. No samples fell completely within the MD range. These domain structure results are typical of fired pottery and indicate their suitability for archaeomagnetic testing. The hysteresis measurements indicate the presence of stable single-domain and pseudo-single domain behavior in all samples, indicating that all samples are suitable for Thellier-style paleointensity experiments.

Figure 8. Domain State of All Samples

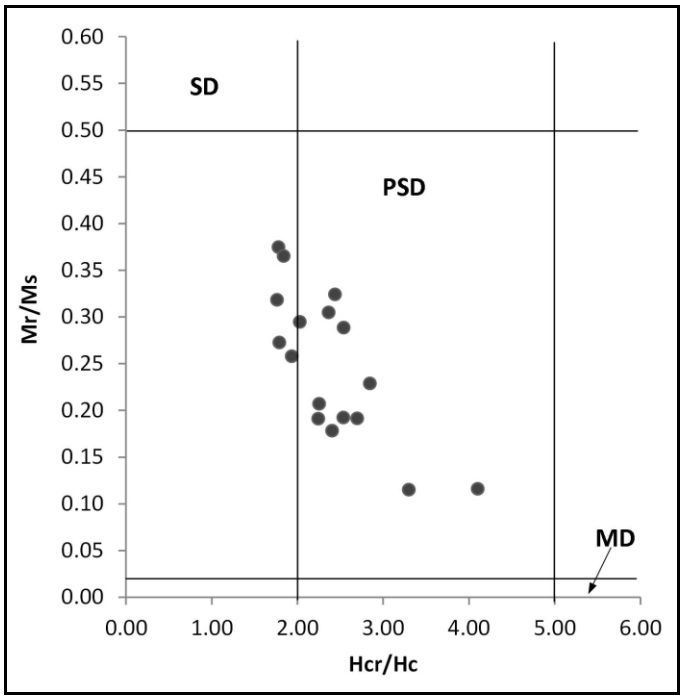

5.3 AF Demagnetization Results

The results of alternating field (AF) demagnetization for four representative specimens are shown in Figure 9, which displays the data following three graphical conventions: normalized NRM AF demagnetization spectra, a stereographic projection, and an orthogonal vector endpoint diagram. Because the samples used in this study represent artifacts not found in their original firing position, they cannot provide magnetic directional data, only intensity. Orthogonal endpoint and stereographic diagrams, which depict magnetic directional information, are utilized here to display the directional trend of the magnetic vector; multiple directions indicating multiple components of remanence. The conventional symbolism for these diagrams has been slightly altered to highlight that they cannot be used to determine the ancient magnetic field direction carried by the samples.

NRM AF demagnetization spectra depict how quickly the samples demagnetize in an applied field. Samples were demagnetized in alternating fields from 2.5 to 170 mT. The spectra for all samples are similar, with an average median destructive field (MDF) of 17 mT (Table B1, Appendix B). Sample 54 (Figure 9d), a modern period grey ware sherd, had the highest MDF at approximately 53 mT. Sample 72, a fully fired, 1 cm thick storage vessel fragment from phase 4, had the lowest MDF at 7 mT. Twelve of the 15 samples contained MDF values higher than 10 mT, indicating that most samples likely contained enough single domain grains to carry a measurable remanence.

Orthogonal projections, or Zijderveld diagrams, display the decay of magnetization as an increasingly large alternating field (or temperature) is applied to the sample. Orthogonal projections display the evolution of the magnetic vector as it decays towards the origin, which is set at the center of a Cartesian coordinate system and corresponds to zero magnetization on the following diagrams. The projections of the NRM vector in the horizontal (H) and vertical (V) plane views are shown as black circles and grey triangles, respectively. The horizontal plane corresponds to declination of the vector from north (or south). The vertical plane corresponds to apparent inclination of the vector, down or up. A single line that decays straight to zero indicates a sample with only one magnetic component.

Specimen 09b (Figure 9a), for example, has only one magnetic component; while specimen 23c (Figure 9b) displays two components of remanent magnetization, causing the vector to initially decay in a different direction, not towards the origin. The smaller secondary component (curved portion of line) for specimen 23c demagnetizes quickly, in the first two low field steps, while the primary component demagnetizes straight to the origin through the majority of the demagnetizing field steps. In this sample, the secondary remanence is considered insignificant and its contribution is removed in final intensity analysis. Specimen 37c (Figure 9c) also has two discrete components of magnetization, which are almost 120° different in their orientation. The secondary component does not fully demagnetize until after a 50 mT field is applied. The primary component dominates for the last seven demagnetization steps. The shape of the vertical orthogonal projection, with an abrupt apparent 90° change between the two components,

indicates that the coercivity distributions of each component do not overlap significantly. This pottery sample may have been reheated to a high temperature, resetting a large majority of the original remanence. This remagnetization may have occurred if the pottery was used as a cooking vessel, or if it was involved in another kind of thermal event like a destructive fire. It also may have been subjected to an IRM, such as a lightning strike, which is plausible since the sample was found in the upper disturbed layer. A third possibility is that the pottery acquired new magnetic minerals via precipitation from iron-rich groundwater. Sample 54c (Figure 9d) also shows two components of remanence in slightly different directions, however, the curved graphs with equally spaced AF steps indicate an increased level of overlap in their coercivity distributions, which makes separating their contributions more difficult.

Stereographic projections also indicate the magnetic direction of remanence, with clusters of overlapping data points indicating stable unidirectional magnetization. Specimen 09b and 23c (Figures 9a and 9b), for example, show a strong single component of magnetization, with all inclinations oriented in the same direction. Samples 37c and 54c (Figures 9c and 9d) display demagnetization data that trace out great circle curves, indicating that the sample contains two magnetization components switching from one direction to the next. Even though several samples showed multiple components of remanence after AF demagnetization, all samples appeared to have one distinguishable primary remanence. Therefore all samples were considered suitable for thermal remanence experiments.

Figure 9. Representative AF Demagnetization Results

Figure 9a. Specimen 09b

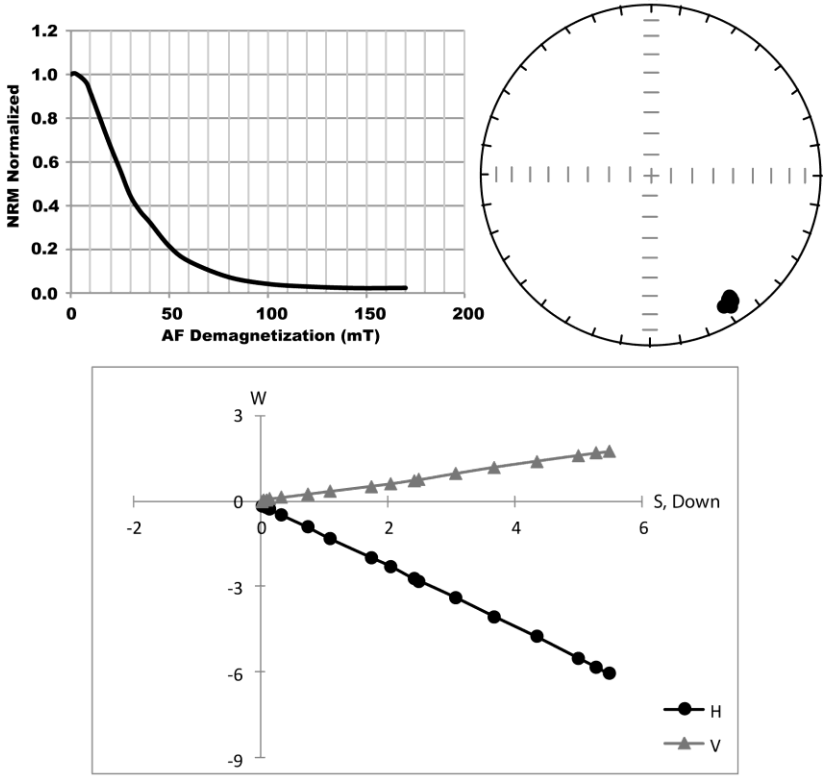

Figure 9b. Specimen 23c

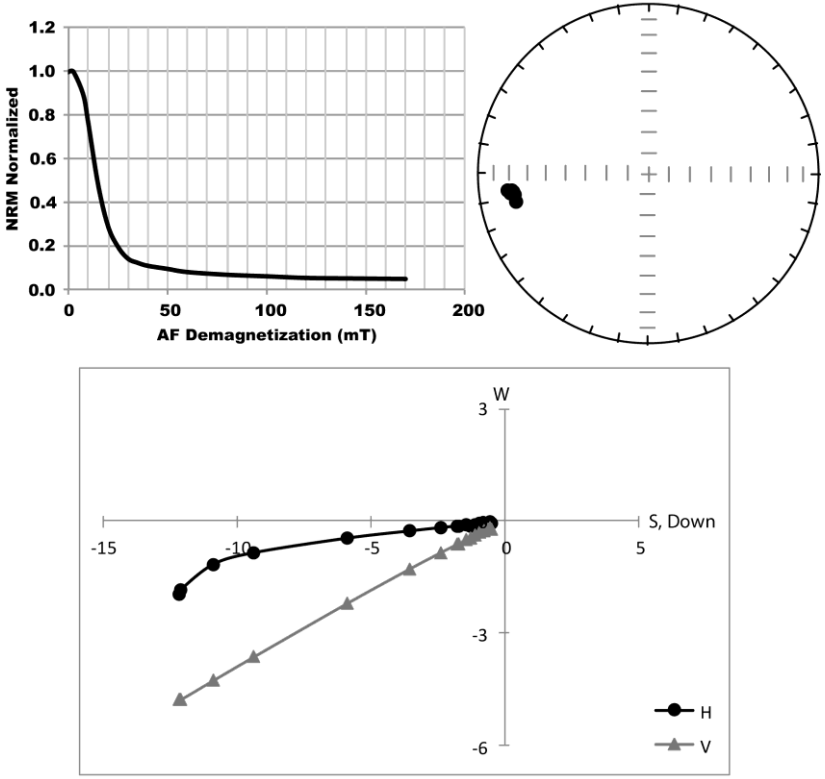

Figure 9c. Specimen 37c

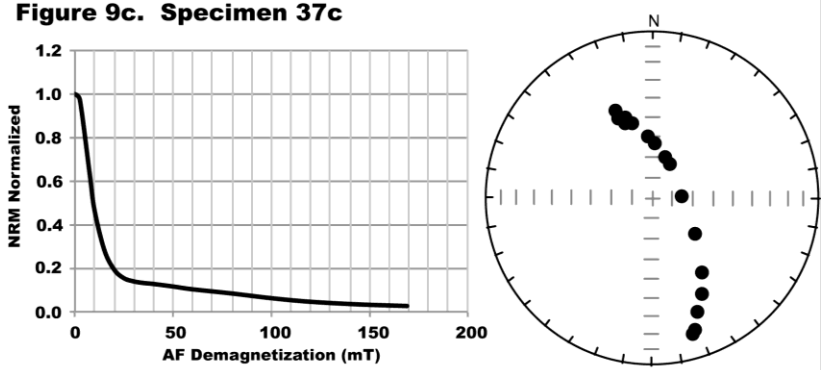

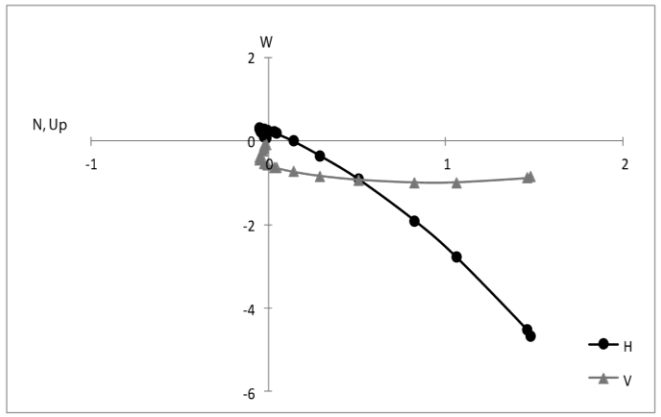

Figure 9d. Specimen 54c

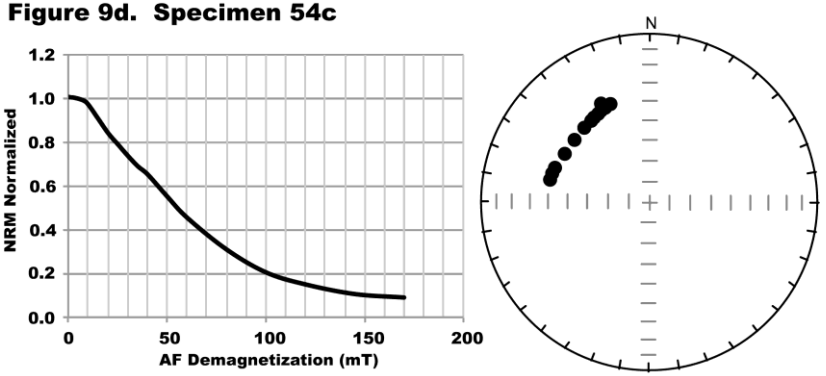

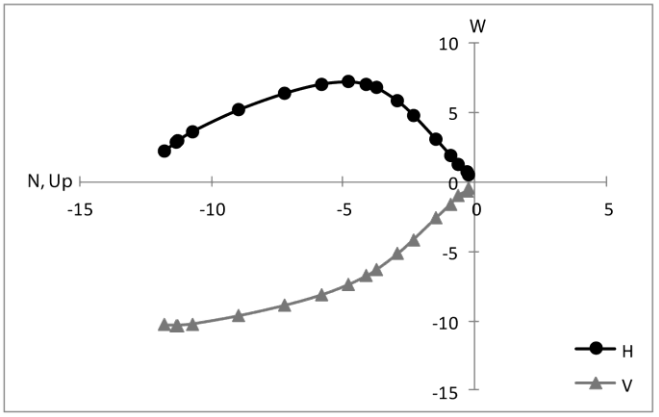

5.4 Thermal Remanent Demagnetization Results

In contrast to many geological samples used in paleomagnetic experiments, fired pottery samples often exhibit a much higher NRM by mass, which may be due to the geological source of the clays or to the deliberate addition of iron-rich tempers. NRM results are listed in Appendix B, Table B1 and range from 1.28 x 10^{-4} Am^2/kg to 1.37 x 10^{-2} Am^2/kg. Specimen set #2 was used in the Thellier-type thermal demagnetization experiments. For all specimens, 95% of the NRM was removed by the 600°C heating step. This indicates that the primary mineral carrying the remanence was likely magnetite or its partially oxidized form, maghemite. Figure 10 displays data from the IZZI paleointensity experiments from three representative specimens. The left-hand plot displays the change in NRM after each heating step. The thin black line is the Vector Difference Sum (VDS) of the NRM demagnetization. The VDS takes into account the various components of magnetization, summing the vector difference at each demagnetization step, resulting in a plot of total magnetization (Tauxe, 2010).

The center graph (Arai plot) displays the NRM lost versus pTRM gained (circles), the results of pTRM checks (squares), and multidomain (MD) checks (triangles). A best-fit line runs through the principal components of magnetization (closed circles) which were used in final intensity calculations. The minimum and maximum temperature endpoints for this line are also listed. The orthogonal vector endpoint diagram (*see section 5.3 for description*) resulting from the thermal demagnetization is displayed to the right.

Figure 10. Representative Thermal Demagnetization Results

Figure 10a. Specimen 09a

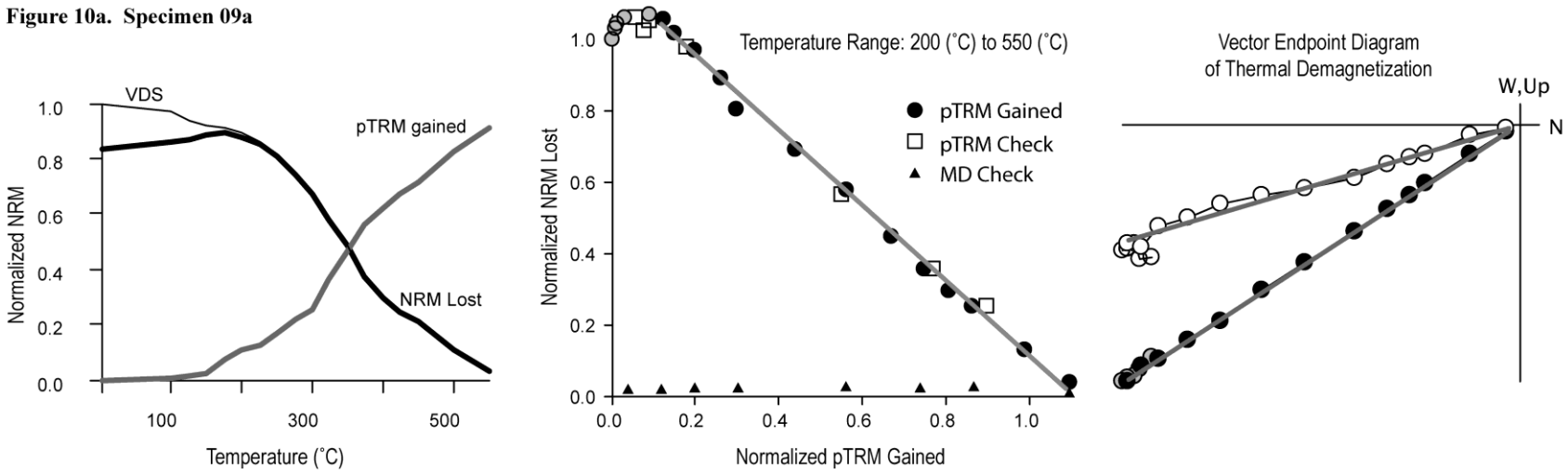

Figure 10b. Specimen 23a

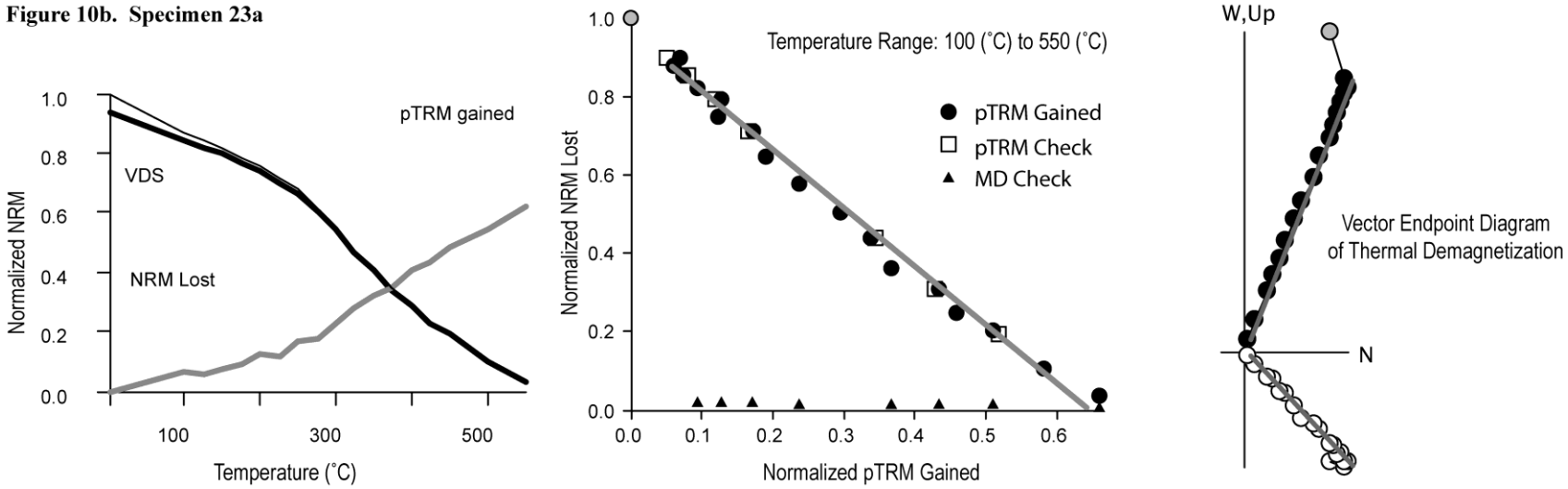

Figure 10c. Specimen 37a

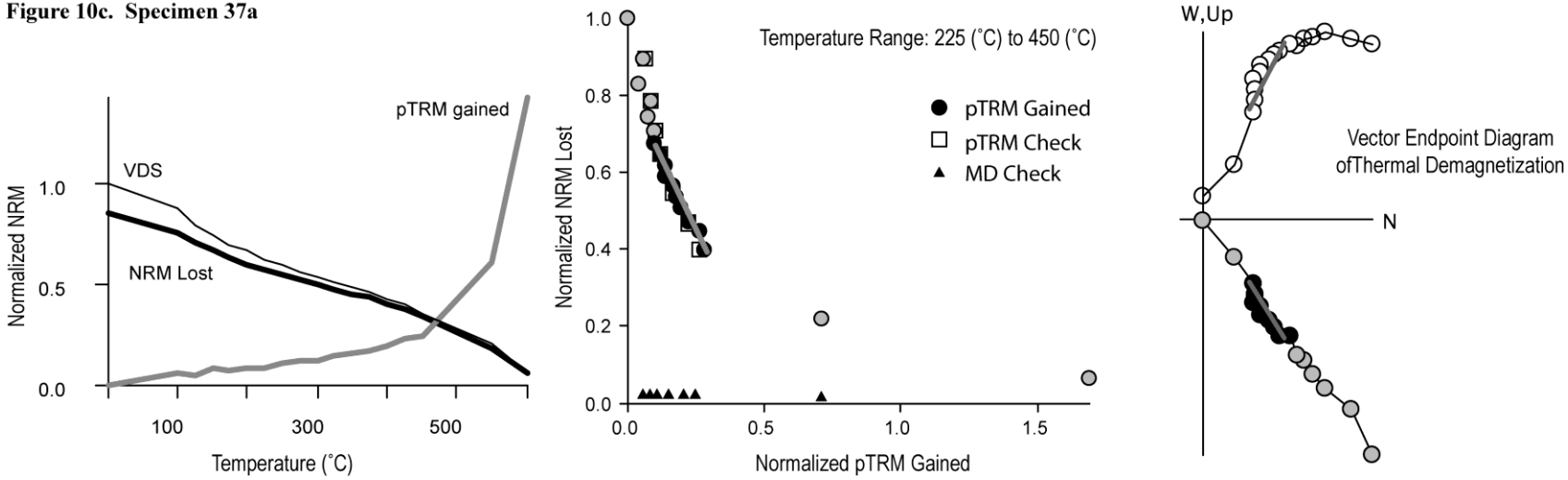

Figure 10b represents an ideal paleomagnetic sample (23a) with one component of magnetization. From the correspondence of pTRM checks with the original heating steps and the steady low value of multidomain (MD) checks it can be inferred that no chemical or domain alteration occurred during heating. Sample 09a (Figure 10a) had a small secondary component of remanence that demagnetized before 200°C and a good correspondence of pTRM checks. Sample 37a (Figure 10c) had more than one component of remanence as noted by the curve or change in direction of the orthogonal endpoint diagrams. The secondary component appears to demagnetize quickly through most of the temperature steps (225-450°C) but gain little pTRM until the final three temperature steps, which represent the primary component of magnetization. This abrupt change in direction from one linear segment of demagnetization to another is in indicator of mineral alteration occurring during the heating process. This sample ultimately failed the quality-control criteria for these paleointensity experiments due to a combination of these factors.

5.5 Archaeointensity (Ba) and Anisotropy (AARM) Results

The linear segment results from each IZZI experiment were used to calculate the final primary field intensity (Ba) recorded by the pottery. Remanence anisotropy was corrected for each sample using anisotropy tensors derived from AARM experiments. Minimum and maximum temperatures and AARM results were calculated using MacThellier software. Final calculations were made in Mathmatica to determine the

acceptance or rejection of results. Results of field intensity calculations sorted by stratigraphic age are summarized in Table 5. Additional results are listed in Table B2, Appendix B.

Table 5. Archaeointensity (Ba) Results

Specimen	Archaeological Date (BCE)	Raw Ba (μT)	Ba AARM Corrected (μT)	Ba error (μT)	VDM (ZAm^2)	VDM error (ZAm^2)
58a	1200-modern	47.5	**56.9**	2.6	102.1	4.7
54a	1200-modern	73.7	**85.8**	13.4	154.0	24.1
9a	1595-1200	31.8	**36.5**	0.6	65.5	1.1
23a	1595-1200	44.5	**49.5**	1.9	88.9	3.4
14a	1900-1595	39.6	**42.2**	2.2	75.7	4.0
13a	1900-1595	42.3	**43.9**	1.2	78.8	2.2
51a	2000-1900	52.1	**54.8**	2.7	98.4	4.8
72a	2112-1900	38.3	**42.3**	3.7	75.9	6.6
32a	2112-1900	50.8	**53.5**	2.5	96.0	4.5
mds04a	2192-2004	36.6	**39.6**	1.3	71.1	2.3
mds01a	2192-2004	47.4	**54.3**	1.9	97.5	3.4
65a	2240-2112	38.9	**44.2**	1.0	79.3	1.8
64c	2240-2112	78.0	**72.9**	15.6	130.9	28
40a	2334-2270	47.6	**44.5**	2.5	79.9	4.5
56a	2334-2270	37.8	**44.5**	0.9	79.9	1.6
37a	unknown	44.6	**45.7**	3.6	82.0	6.5
35c	unknown	48.2	**49.6**	1.1	89.0	2.0

Ba is intensity in μT, VDM is Virtual Dipole Moment in $Am^2 \times 10^{22} (ZAm^2)$

Using principal component analysis, the following criteria were set as thresholds for accepting or rejecting paleointensity values. Results for these values can be found in Table B2, Appendix B. The Maximum Angular Deviation (MAD) represents the variance of the points within a particular temperature interval used to define the best-fit direction. Values above 8° were rejected. The Deviation Angle (DANG) is the angle between the

best-fit line connecting the data to the origin and the best-fit line through the data (Tauxe, 2010). If this angle was greater than 5° then the sample failed. Fvds is the fraction of magnetization normalized by the vector difference sum (vds) of the NRM used to calculate the slope of the line that defines the intensity. Values below 0.6 were rejected. Of the seventeen samples used in this research, only two failed final acceptance criteria for intensity calculations, samples 37 and 64 (see Table B2, Appendix B). This represents a success rate of 88%, higher than previously published research with similar sample numbers. Sample 54 had an unusually high error rate but did not fail acceptance criteria.

Section 6. Discussion

6.1 Construction of Preliminary Archaeointensity Dating Curve

According to Gallet et al. (2008 & 2006), Gallet and LeGoff (2006), and Genevey et al. (2003), the magnetic field intensity for Syria mirrors that for the surrounding region including Egypt, Israel, Jordan, Greece, and Georgia. Including archaeointensity data from the surrounding region, therefore, can result in a more rigorously constructed archaeointensity curve. While the data from Egypt and Georgia appears to follow the Syrian curve data closely (Genevey et al., 2003), they are not included in this initial curve construction in order to compare the Tell Mozan results to data localized to the immediate area surrounding and including Syria. Figure 11 displays the localized curve constructed for Syria. The data used in this curve construction were selected from post-1980 data published to the GEOMAGIA database and constrained to the area encompassing 29°N to 39°N and 32°E to 46°E (an approximate radius of 500 km from central Syria). This region results in 100 archaeointensity data points for Cyprus, Iraq, Israel, Jordan, and Syria. Additional data for Syria (Gallet et al., 2008) was also included in the construction of the curve. The different research sources are highlighted by different symbols on the curve. Research by Aitken et al. includes intensity values for Syria, Cyprus, Israel, and Iraq (1984 and 1989). Walton's 1990 research results include intensity values for Crete. Archaeointensity research based on copper slag analysis in Jordan and Israel (Ben-Yosef et al., 2008 and 2009) is combined as an open circle symbol and the previous Syrian

research data outlined in section 2.4 is combined as open squares. Tell Mozan samples with known archaeological age were plotted after curve construction (closed circles). Horizontal error bars represent the maximum and minimum extent of the archaeological defined dates for each point, which is plotted at the median age. Vertical error bars represent the one-sigma error of the intensity values. A linear best-fit model of the data for this and subsequent curves was constructed using a ninth order polynomial (Appendix B, Table B4). The shaded region around the curve represents the one-sigma error envelope about the model. A simplified version of this preliminary curve displaying only the Mozan data points in relation to the curve is shown in Figure 12.

Figure 11. Preliminary Archaeointensity Dating Curve for Syria

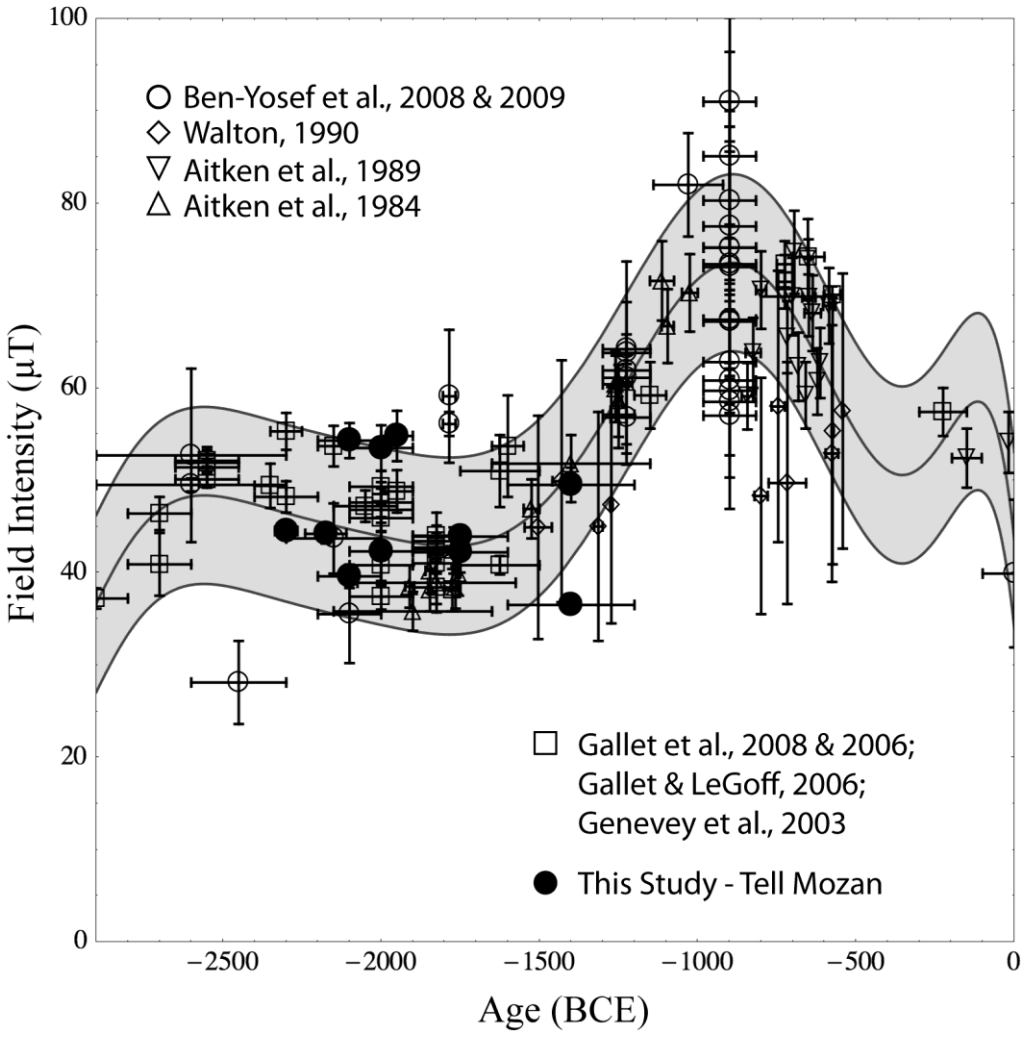

6.2 Estimated Age of Tell Mozan Samples of Unknown Archaeological Age

Two samples from this study are not plotted in the preliminary curve: Samples 37 and 64, which were rejected based on their intensity results. Additionally, samples 54 and 58, which are associated with phase 7 (1200 BCE to modern), and sample 35 with no known age, are excluded. In order to determine the likely archaeomagnetic date for these

three samples, their respective intensities are plotted as dashed lines on Figure 12. The potential archaeomagnetic dates for these three samples corresponds to where the dashed lines cross the dating curve.

Samples 58 yielded an intensity result of 56.9 ± 2.6 μT, which falls across two points on the curve, approximately 1350 BCE and 550 BCE, and in the error envelope associated with approximately 2600 to 2400 BCE. Sample 58 is associated with phase 7 (1200 BCE to modern), which would indicate that the dates of 1350 BCE and 550 BCE may be equally accurate. Recent communications with E. Frahm and M. Kelly-Buccellati revealed that sample 58 came from a gully feature that contained samples from several older phases and possibly spoils from previous excavations. Sample 58 represents an unusual pottery style for Mozan, one Buccellati notes is only associated with phase 4 (2112-1900 BCE). However, the high intensity value for this sample does not fall within the error envelope for phase 4, although it falls close to the acceptable error range for phase 3 and close to the acceptable error for 2400 BCE.

Figure 12. Mozan Data in Comparison to Preliminary Curve

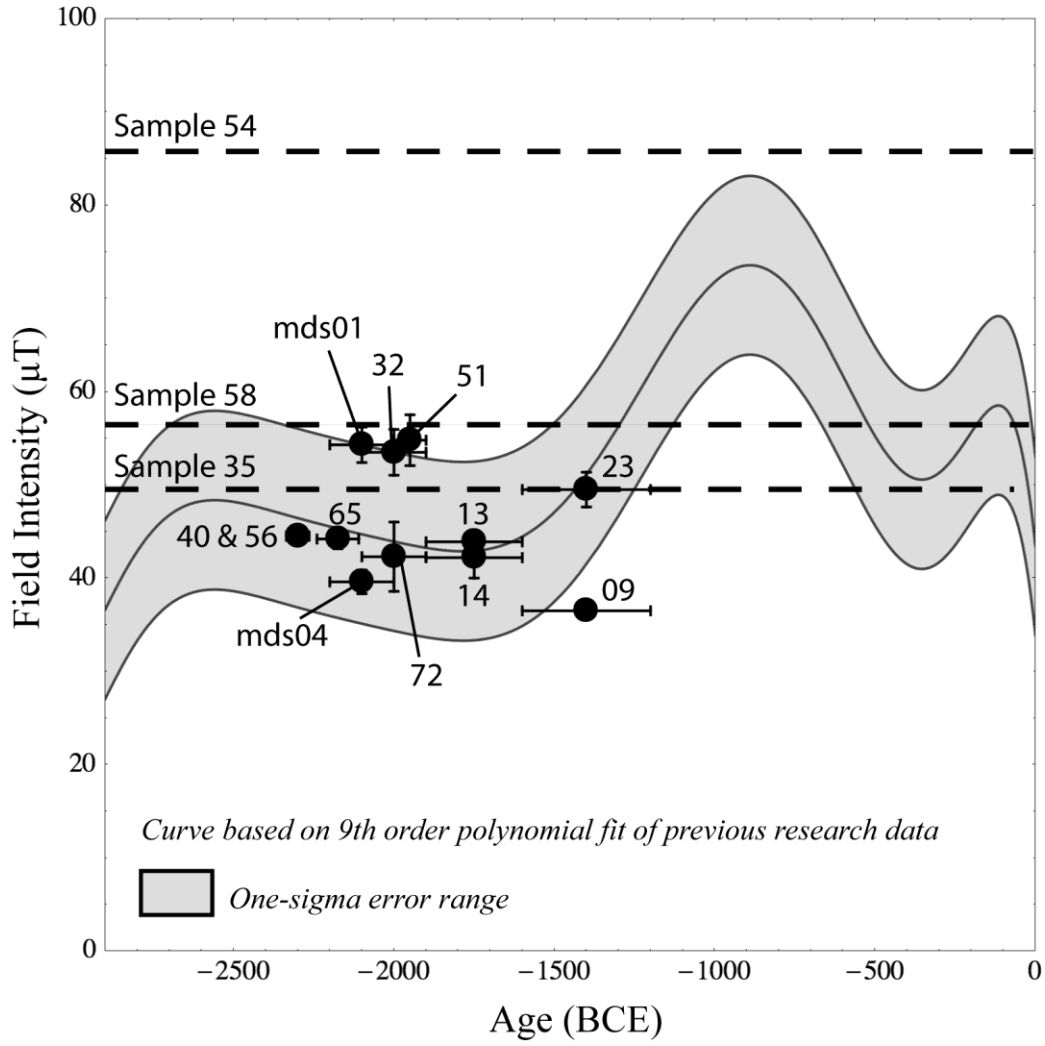

Sample 54 also from phase 7, had the highest intensity value of 85.8 ± 13.4 μT. Based on the sample's error rate, it falls within the error envelope for 1150 to 750 BCE and appears to correspond with other archaeomagnetic data from 900 BCE (Figure 11), a period where a spike in intensity occurred as documented by Ben-Yosef et al. (2008 & 2009). This period represents the highest regional intensities measured in all previous

archaeomagnetic research. Analysis of all studies recorded by the GEOMAGIA database indicate that intensity continued to decrease after 900 BCE through the 20th century AD, therefore it is unlikely the sample is from a later date.

Sample 35 yielded an intensity of 49.6 ± 1.1 μT, placing probable age between 2500 BCE and 1400 BCE on the curve. Recent correspondence with M. Buccellati resulted in a determination that the piece came from phase 3, placing its archaeologically defined age between 2240 and 2112 BCE, which corresponds to the possible archaeomagnetic dates for the sample's intensity.

6.3 Preliminary Archaeointensity Dates for Samples of Known Archaeological Age

Sample 40 and 56, from phase 1 (2334-2270 BCE), resulted in nearly identical intensity results (44.5 ± 2.5 and 44.5 ± 0.9 μT, respectively), which would be expected from similar ware types located in the same stratigraphic layer. These samples place very well on the intensity curve for their archaeologically determined date (Figure 12). Sample 65, archaeologically dated to phase 3 (2240-2112 BCE), resulted in a similar intensity value and appears to correspond to an archaeointensity date of approximately 2150 BCE.

Samples mds01 and mds04 originated from a pit structure filled with debris that was archaeologically determined to be of phase 3b to phase 4 origins (2192-1900 BCE). These two samples yielded extremely different intensities, 54.3 ± 1.9 and 39.6 ±1.3 μT, respectively. Sample mds04 more closely matches the intensity curve dates

corresponding to phase 4 (2112-1900 BCE), while sample mds01 falls on the edge of the one-sigma error range for phase 3b (2192-2112 BCE). The unusually high intensity for sample mds01 may indicate that it originates from an earlier phase, around 2400 BCE. Because phases 3 and 4 fall in a period of intensity decline that occurred after 2500 BCE, it is possible that sample mds04 originated from the later part of phase 4, around 2000 BCE and sample mds01 from their earlier part of phase 3b, around 2190 BCE.

Samples 32 and 72, date to phase 4, and similar to mds01 and mds04, have variable intensities. Sample 32 more closely matches sample mds01, falling on the edge of the one-sigma error envelope with a high intensity of 53.5 ± 2.5 μT. Again, this high intensity places its likely date closer to 2112 BCE on the curve and possibly older. Sample 72, has an intensity of 42.3 ± 3.7 μT, placing very well on the intensity curve and dates very close to 2000 BCE. Sample 51, from phase 4b (2000-1900 BCE), had a similar intensity (54.8 ± 2.7 μT) as samples mds01 and 32. This sample's intensity is slightly high for the archaeologically determined phase dates, and barely falls within the one-sigma error envelope based on its error range, indicating it is possibly older than phase 4b, and certainly no younger than 2000 BCE.

Sample 13 and 14 from phase 5 (1900-1595 BCE) yielded similar results, 43.9 ± 1.2 and 42.2 ± 2.2 μT, respectively. This time period is characterized by a "valley" of low intensity: a decrease in intensity that occurred between 1900 and 1700 BCE before a rapid increase in intensity that lasted until approximately 900 BCE. The median archaeological age for samples 13 and 14 falls right on the predicted archaeomagnetic age of 1750 BCE based on their intensity.

Samples 23 and 9 from phase 6 (1595-1200 BCE) differed by 13 μT, with sample 9 having an intensity of 36.5 ± 0.6 μT, the lowest of all samples. This low intensity value appears to correspond to the intensity valley that occurred around 1700 BCE. However, sample 9 still falls within the error envelope and, therefore, most likely originates from the earliest dates in phase 6, approximately 1595 to 1500 BCE. Sample 23 (49.5 ±1.9 μT) matches the intensity curve perfectly for 1400 BCE, its median archaeological age.

6.4 Comparison of Mozan Results to Greater Regional Curve

In order determine if the addition of data from more distant neighboring regions will modify the results, an additional 120 data points were added in order to create a larger regional curve (Figure 13). This curve represents a region with a radius of approximately 1300 km from central Syria and includes additional intensity results from Egypt, all of Greece including the Cycladic Islands, Cyprus, and all of Israel, Jordan, and Iraq. This new curve is also expanded back to 4000 BCE. Comparison of Figures 11 and 13 shows no appreciable difference between the two curves or the placement of the Tell Mozan results with the exception of samples mds01, 32, 51, and 58. Sample 58, assigned to phase 4, again falls outside the error envelope, and 51, which barely fell within the error envelop in the preliminary curve, completely falls out of the one-sigma error envelope on the expanded curve (Figure 13). Samples 32 and mds01 also shift, falling on the very edge of the acceptable error. These four samples appear to have significantly higher intensities than the curve predicts for the period between 2200 and 1900 BCE, and

therefore, may be much older than archaeologically defined. Because sample 58 originated from a mixed stratigraphic context, it cannot be definitively dated archaeologically and will not be considered in the final new Syrian curve construction. Sample 51 will also be excluded. The remaining eleven samples displayed more accurate age results with this expanded intensity curve.

Figure 13. Greater Regional Archaeointensity Dating Curve

(Cyprus, Egypt, Greece, Jordan, Iraq, Israel, and Syria)

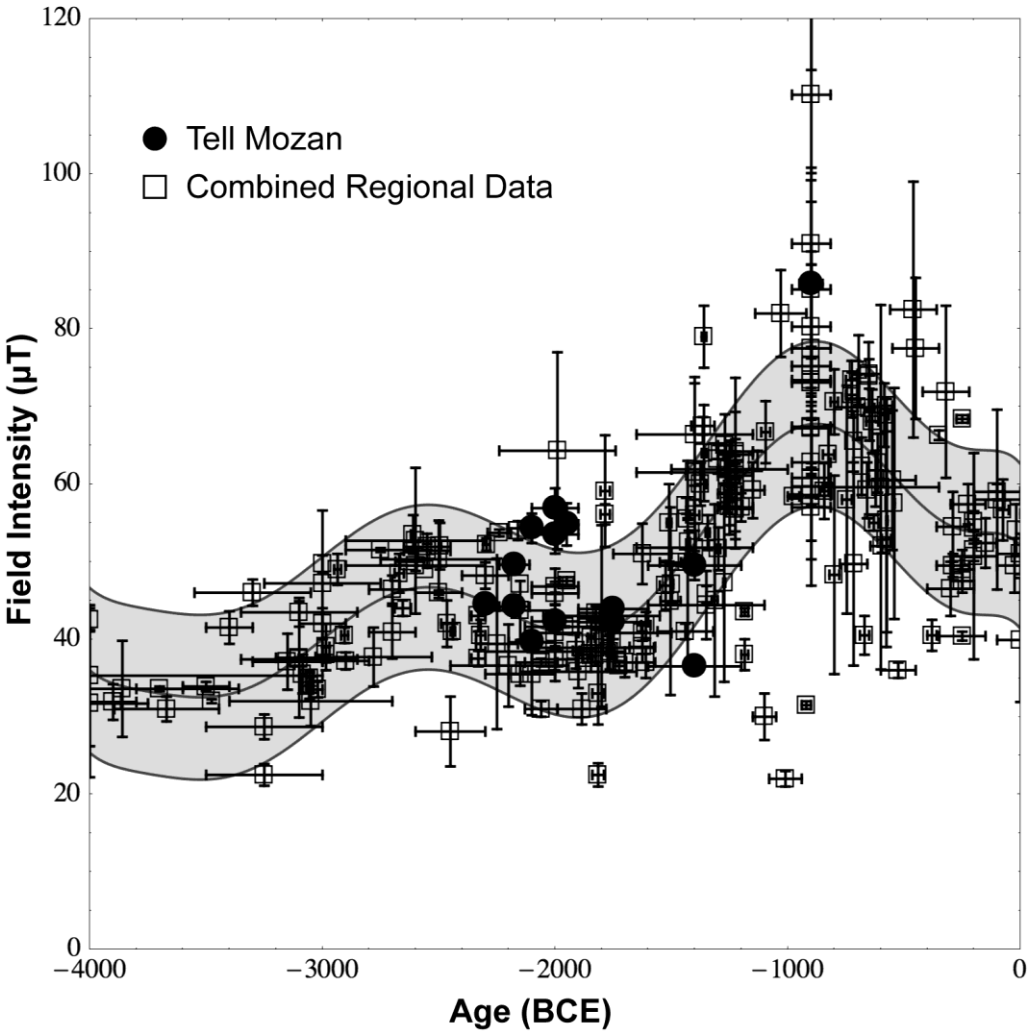

6.5 Comparison of Relative and Archaeomagnetic Dates for Tell Mozan

Table 6 compares the archaeologically determined relative dates for all samples and the final dates determined from archaeomagnetic dating. The final archaeomagnetic date is based on intensity values only and the final placement of Tell Mozan samples on the greater regional curve model (Figure 13). In most instances, the narrowest range for possible archaeomagnetic dates corresponds with the range for archaeological dates, with the exception of four samples, mds01, 32, 9, and 54. The archaeomagnetic ages are much narrower for these four samples.

Of the seventeen total samples, only two failed archaeointensity experiments. Of the remaining fifteen samples, ten corresponded extremely well with their archaeological dates and three fell within the acceptable error range for their archaeologically defined dates. These three samples, mds01, 32, and 9, most likely correlate with their oldest archaeological dates and may actually be slightly older. Sample 54 most likely dates between 1150 and 75 BCE and strongly matches the intensity spike identified for 950 BCE. However, this sample came from phase 7, which represents an infinitely broad span of time (1200 to modern). While the average intensity of the Earth is known to have decreased since 950 BCE, intensities do fluctuate at small scales, and sample 54 could feasibly represent another more recent date, therefore, it was not included in the final Syrian curve construction (Figure 14). The final two samples, 51 and 58, statistically fall outside their archaeologically defined dates and are also not included in the final curve. The high intensity of both samples indicates a date at least 200 years older than

archaeologically defined or possible evidence of an additional spike in intensity during this period that was not previously recorded.

Table 6. Comparison of Relative and Archaeomagnetic Dates for Tell Mozan

Sample ID	Site Phase	Archaeological Date (BCE)	Archaeomagnetic Date (BCE)
40	1	2334-2270	2334-2270
56	1	2334-2270	2334-2270
35	3	2240-2112	2240-2112
64	3	2240-2112	*Failed*
65	3	2240-2112	2240-2112
mdS01	3b/4	2192-2004	**2192-2100**
mdS04	3b/4	2192-2004	2192-2004
32	4	2112-1900	**2112-2100**
58	4	2112-1900	2400-2200*
72	4	2112-1900	2112-1900
51	4b	2000-1900	2400-2200*
13	5	1900-1595	1900-1595
14	5	1900-1595	1900-1595
9	6	1595-1200	**1595-1500**
23	6	1595-1200	1595-1200
54	7	1200-modern	*950 ±200*
37	7	1200-modern	*Failed*

** Sample falls outside of its relative dating range, likely date listed. Bolded date indicates that sample likely dates closer to one end of its archaeomagnetic date range.*

6.6 Final New Archaeointensity Dating Curve for Syria

Based on the results of archaeomagnetic measurements and cross-correlation with the greater regional curve (Figure 13), a final refined curve for Syria was constructed

incorporating the results from this study and the data used to construct Figure 13. This curve represents over 230 data points and covers an area with a radius from central Syria of approximately 1300 km (Figure 13). Samples 37, 64, 58, 51, and 54 were not included in this final curve construction.

Figure 14. New Archaeointensity Dating Curve for Syria

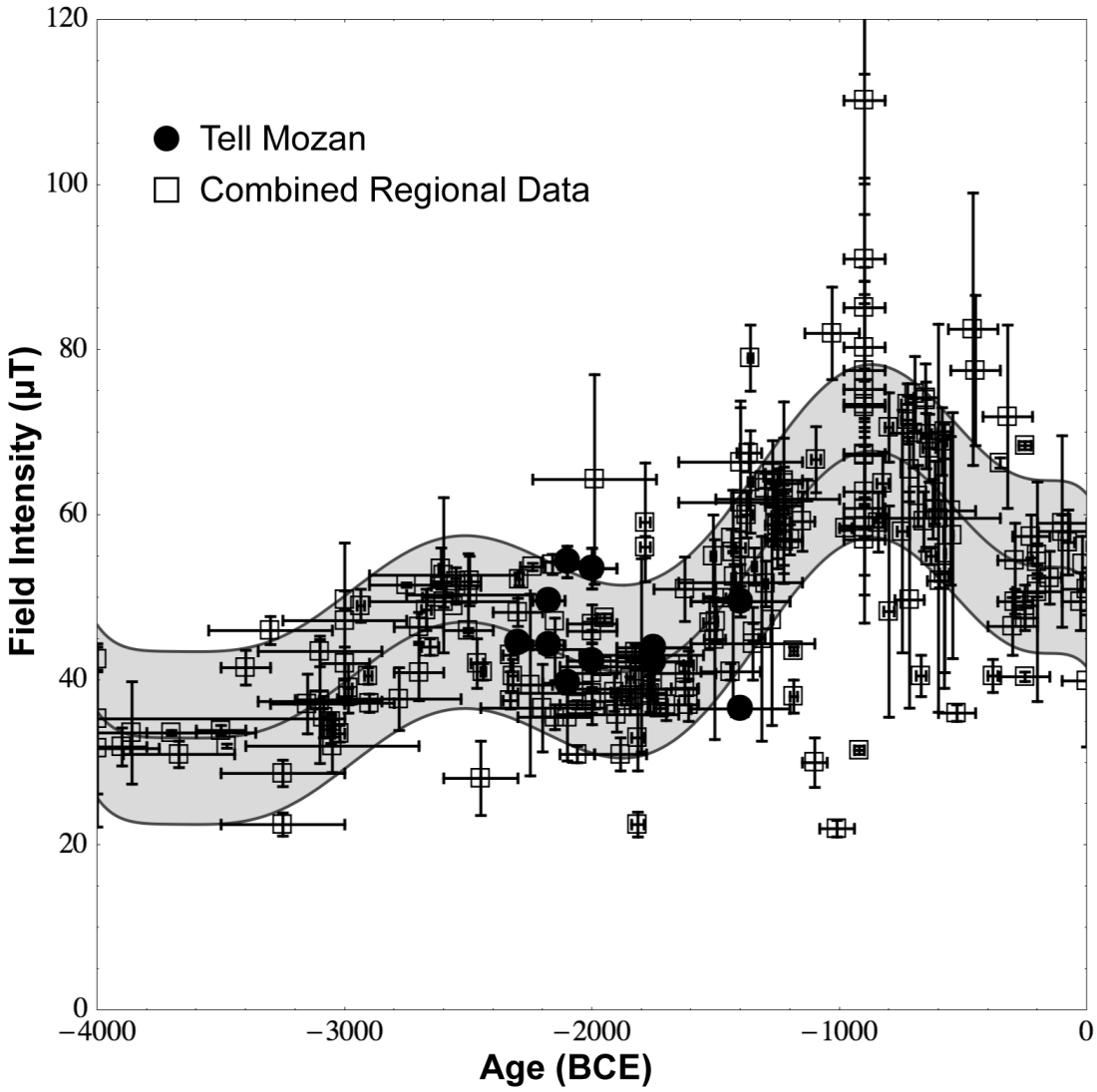

6.7 Sources of Dating Discrepancies

While the majority of samples resulted in highly correlated results between archaeomagnetic and archaeological dates, potential sources for the discrepancies in the samples that did not correspond well should be considered.

Despite careful excavation, misidentifications of both artifacts and features can occur in the field. For example, sherds from later strata can become dislodged from trench walls, especially in dry climates, contaminating earlier stratigraphic levels. Samples mds01 and mds04 were found in a pit, a type of feature that often intersects more than one stratum. This particular feature contained artifacts associated with phase 4, but measurements from these two samples exhibit quite different intensities that do not correspond well with a single phase. This result suggests that samples from pits or other mixed or disturbed features should be avoided. Disturbed layers may also include destruction layers, in which artifacts may have been subjected to intense fires that reset their remanent magnetizations. None of the samples in this study, however, appear to come from such an event.

Discrepancies may also represent contamination that occurred in antiquity. For example, materials such as old sherds and brick from one part of the site may have been used as fill for later constructions. There are examples of this practice at Tell Mozan, such as the use of Late Chalcolithic fill to build up the Early Bronze Age temple terrace.

Unusual intensity results may also indicate that artifacts originate from another region with a different range of magnetic intensities. Studies of the obsidian artifacts

from Phase 2, circa 2300-2200 BCE, reveal that seven different obsidian sources are represented at the ancient city, including a Central Anatolian source that suggests the Urkesh inhabitants were engaged in a long-distance exchange that linked them to the Aegean (Frahm and Feinberg, 2013). Additionally, during this period, red-and-black burnished sherds characteristic of the Early Transcaucasian or Kura-Araxes complex are found in palace and temple strata, attesting to trade links as far northeast as the South Caucasus (Frahm, 2010). Sample 58 may have been such a piece. Thus, not all sherds at the site are local, and even if the phases are well-defined, sherds could be from pots manufactured elsewhere.

Furthermore, the sherds in this study were not originally collected or exported with archaeomagnetic studies in mind. This did not affect the actual measurements; however, sample section was limited by the need for a necessary sample size for experiments. As a result, a few samples with less than ideal feature associations were included. Measuring greater numbers of samples from each stratum or feature may have yielded improved correlations.

The most striking results of this study were the number of samples archaeologically dated to the period between 2100 and 2000 BCE that appeared to have an unusually high intensity. If these samples were correctly dated archaeologically, these results could indicate the presence of a previously unidentified magnetic jerk or spike during this period. Additional testing of samples from this period, may clarify this issue.

Section 7. Conclusion

The results of this study indicate that archaeomagnetic dating can be used as a complementary absolute dating tool in archaeological research. Final archaeointensity results for all seventeen pottery samples in this research resulted in an 88% success rate in archaeomagnetic experiments. Of the fifteen samples that returned acceptable intensity results, nine coincided very well with their archaeologically determined dates, three were statistically acceptable and two fell outside the one-sigma error envelope. The final sample, 54, could not be definitively dated. Working under the assumption that the archaeologically derived relative dates for Tell Mozan were correctly defined for the samples, this resulted in an overall success rate of 71% for all samples. The final results of magnetic mineral characterization tests and archaeointensity experiments indicate that a variety of pottery ware types can be used in archaeomagnetic dating, with the possible exception of grey wares which may not be fully oxidized and may not have been heated above the Curie temperature of their constituent magnetic minerals. Of the two grey ware sherds tested, one failed the acceptance criteria for intensity values and the other resulted in an unusually high intensity error rate. Neither sample was included in the final Syrian curve construction, however, it should be noted that the latter sample was not included based on its poorly defined archaeological date, not on its intensity results. Further testing of grey ware type pieces may indicate whether these types of wares are indeed unsuitable for archaeomagnetic experiments.

This new archaeointensity data from Tell Mozan augments and improve existing

global and regional archaeomagnetic databases for the periods between 2350 and 1200 BCE. The results of this and previous studies highlight the need for additional archaeomagnetic measurements on samples from 2500-2000 BCE in order to determine the peak intensity during that time period. Four of the six samples from Tell Mozan that archaeologically date to phase 3b and 4 (2192-1900 BCE) seem to have much higher intensity values than would be expected, indicating they may be associated with much older dates (2400-2200 BCE) or that this time period may contain a geomagnetic spike not previously recorded. The former is more likely as two of the four samples came from disturbed or pit features where intermixing of various phase debris may have occurred. Reanalysis of these features or further testing on phase 3b and 4 samples is warranted.

Finally, it is important to note that the results obtained from this study can also be utilized to answer additional archaeological questions. The identification of multiple components of remanence in some of the pottery sherds may indicate that the pottery was reheated at lower temperatures, information that can be used by domestic archaeologists studying cooking vessels or those investigating the ritual use of ceramics. A possible future study could be the comparison of the kinds of wares that are used to determine archaeomagnetic dates. For example, objects created for one-time use, such as burial offerings, or domestic ceramics with a short life span due to breakage, may be more likely to accurately date to the time of their manufacture. Archaeointensity results that do not correspond well with relatively dated ceramics may be proof of long distance trade or the careful and continued use of certain objects, possibly those with ritual or sentimental value. In some cases, unusual intensity values in random sherds may also indicate that

very old broken pottery or previous settlement debris is being recycled into new building materials or foundations.

The techniques used in this study can also be applied to fired mudbrick, metal slag, burnt soils and rock, hearths, and clay ovens. Objects found *in-situ* can yield valuable magnetic directional data, which can be used to calibrate existing dating curves. Destructive fires or other burning events may record a magnetic remanence in soils and destruction debris, helping researchers to identify historic events. Magnetic remanence in metal slags, ovens, kilns, and hearths can help identify last use of a site. For some regions, the narrowing of possible site dates through archaeomagnetic dating may answer questions regarding political control and timing of cultural change. This is especially relevant at sites like Tell Mozan and others in the region with a long history of reuse by peoples from different cultures or economic strategies. Therefore, archaeomagnetic dating is not merely an important chronological tool, but provides valuable data that can be used in further archaeological investigation.

References

Aitken, M.J., Allsop, A.L., Bussell, G.D., Gillian, D.,Winter, M.B., 1989. Geomagnetic intensity variation during the last 4000 years. *Physics of the Earth and Planetary Science 56,* 49-58.

Aitken, M.J., Allsop, A.L., Bussell, G.D., Winter, M.B., 1984. Geomagnetic intensity in Egypt and western Asia during the second millennium BC. *Nature* 310, 26, 306-308.

Aitken, M.J., Weaver, G.H., 1962. Magnetic dating: some archaeomagnetic measurements in Britain. *Archaeometry* 5, 4-22.

Anthavale, R.N., 1969. Intensity of the geomagnetic field in prehistoric Egypt. *Earth and Planetary Science Letters* 6, 221-224.

Banerjee, S.K., Mellema, J.P., 1974. A new method for the determination of paleointensity from the A.R.M. properties of rocks. *Earth and Planetary Science Letters* 23, 2, 177-184.

Ben-Yosef, E., Tauxe, L., Levy, T.E., Shaar, R., Ron, H., Najjar, M., 2009. Geomagnetic intensity spike recorded in high resolution slag deposit in southern Jordan. *Earth and Planetary Science Letters* 287, 529-539.

Ben-Yosef, E., Ron, H., Tauxe, L., Agnon, A., Genevey, A., Levy, T.E., Avner, U., Najjar, M., 2008. Application of copper slag in geomagnetic archaeointensity research. *Journal of Geophysical Research* 113, doi:10.1029/2007JB005235.

Ben-Yosef, E., Tauxe, L., Ron, H., Agnon, A., Avner, U., Najjar, M., Levy, T.E., 2008. A new approach for geomagnetic archaeointensity research: insights on ancient metallurgy in the southern Levant. *Journal of Archaeological Science* 35, 12, 2863-2879.

Buccellati, G., 2007. *2007 Excavations at Tell Mozan, ancient Urkesh and plans for 2008*. The International Institute for Mesopotamian Area Studies.

Buccellati, G., 2005. *Tell Mozan Urkesh: special topics*. The International Institute for Mesopotamian Area Studies.

Buccellati, G., 2003. *Urkesh chronology*. Website: http://128.97.6.202/urkeshpublic/chronology.htm Last accessed 5/29/12.

Buccellati, G.., Kelly-Buccellati, M., 2005. Urkesh as a Hurrian religious center. *Studi Micenei ed Egeo-Anatolici* 47, 27-59.

Bucha, V., Mellaart, J., 1967. Archaeomagnetic intensity measurements on some Neolithic samples from Çatal Hüyük (Anatolia). *Archaeometry* 10, 23-25.

Burlatskaya, S.P., Nachasova, I.E., Nechaeva, T.B., Rusakov, O.M., Zagniy, G.F., Tarhov, E.N., Tchelidze, Z.A., 1970. Archaeomagnetic research in the U.S.S.R.: recent results and spectral analysis. *Archaeometry* 12, 73-85.

Butler, R.F., 1992. *Paleomagnetism: Magnetic domains to geologic terranes*. Blackwell Scientific Publication, United States.

Chauvin, A., Garcia, U., Lanos, Ph., Laubenheimer, F., 2000. Paleointensity of the geomagnetic field recovered on archaeomagnetic sites from France. *Physics of the Earth and Planetary Interiors* 120, 111-136.

Coe, R.S., Grommé, S., Mankinen, E.A., 1978. Paleointensities from radiocarbon-dated lava flows on Hawaii and the question of the Pacific nondipole low. *Journal of Geophysical Research* 83, 1740-1756.

Courtillot, V., and Le Mouël, J.L., 2006. The study of the Earth's magnetism (1269-1950): A foundation by Peregrinus and subsequent development of the geomagnetism and paleomagnetism. *Reviews of Geophysics*, 45, RG3008, doi:10.1029/2006RG000198.

Day, R., Fuller, M.D., and Schmidt, V.A., 1977. Magnetic hysteresis properties of synthetic titanomagnetites. *Physics of the Earth and Planetary Interiors* 13, 260-266.

Donadini, F., Korhomen, K., Riisager, P., and Pesonen, L., 2006. Database for Holocene geomagnetic intensity information. *EOS, Transactions, American Geophysical Union* 87(14), 137.

Dunlop, D. J. and Özdemir, Ö., 1997. *Rock Magnetism: fundamentals and frontiers.* Cambridge University Press, UK.

Dyson Jr., R. J., 1968. *The Archaeological Evidence of the Second Millennium B.C. on the Persian Plateau.* Vol. II, Chapter XVI in: The Cambridge Ancient History Series. UK: Cambridge University Press.

Eighmy, J.L., 1990. Archaeological dating: practical problems for archaeologists, in: J.L. Eighmy, J.L., Sternberg, R.S. (Eds.), *Archaeomagnetic Dating*. University of Arizona Press, Tucson, pp. 33-64.

Frahm, E., 2010. *The Bronze-Age Obsidian Industry at Tell Mozan (Ancient Urkesh), Syria: Redeveloping Electron Microprobe Analysis for 21st-Century Sourcing Research and the Implications for Obsidian Use and Exchange in Northern Mesopotamia after the Neolithic.* University of Minnesota Dissertation, MN.

Frahm, E. and Feinberg, J.M., 2013. Environment and collapse: Eastern Anatolian obsidians at Urkesh (Tell Mozan, Syria) and the third-millennium Mesopotamian urban crisis. *Journal of Archaeological Science*, 40, 4, 1866-1878.

Gallet, Y., Le Goff, M., Genevey, A., Margueron, J., Matthiae, P., 2008. Geomagnetic field intensity behavior in the Middle East between 3000 BC and 1500 BC. *Geophysical Research Letters* 35, L0237, doi:10.1029/2007GL031991.

Gallet, Y., Genevey, A., Le Goff, M., Fluteau, F., Eshraghi, S., 2006. Possible impact of the Earth's magnetic field on the history of ancient civilizations. *Earth and Planetary Science Letters* 246, 17-26.

Gallet, Y., Le Goff, M., 2006. High-temperature archaeointensity measurements from Mesopotamia. *Earth and Planetary Science Letters*, 241, 159-173.

Genevey, A., Gallet, Y., Margueron, J., 2003. Eight thousand years of geomagnetic field intensity variations in the eastern Mediterranean. *Journal of Geophysical Research* 108, No. B5, 2228, doi:10.1029/2001JB001612.

GEOMAGIA50, 2011. Scripps Institution of Oceanography, University of California, San Diego. Website: http://geomagia.ucsd.edu/geomagia Last accessed: 1/10/13.

Korhonen, K., Donadini, F., Riisager, P., and Pesonon, L., 2008. GEOMAGIA50: an archaeointensity database with PHP and MySQL. *Geochemistry, Geophysics, Geosystems* 9, doi:10.1029/2007GC001,893.

Korte, M., Constable, C., Donadini, F., Holme, R., 2011. Reconstructing the Holocene geomagnetic field. *Earth and Planetary Science Letters* 312, 497-505.

Kovacheva, M., Spartharas, V., Liritzis, I., 2000. New archaeointensity results from Greek materials. *Archaeometry* 42, 2, 415-429.

Kovacheva, M., 1997. Archaeomagnetic database from Bulgaria: the last 8000 years. *Physics of the Earth and Planetary Interiors* 102, 145-151.

Leonhardt, R., Saleh, A., Ferk, A., 2010. Archaeomagnetic field intensity during the Roman Period at Siwa and Bahryn Oasis, Egypt: implications for the fidelity of Egyptian archaeomagnetic data. *Archaeometry* 52, 3, 502-516.

Lanos, P., Le Goff, M., Kovacheva, M., Schnepp, E., 2005. Heirarchical modeling of archaeomagnetic data and curve estimation by moving average technique. *Geophysics Journal International* 160, 440-476.

Lodge, A., Holme, R., 2008. Towards a new approach to archaeomagnetic dating in Europe using geomagnetic field modeling. *Archaeometry* 51, 2, 309-322.

Moskowitz, B., 1991. *Hitchhiker's Guide to Magnetism*. Institute for Rock Magnetism, University of Minnesota. Website: http://www.irm.umn.edu/hg2m/hg2m_index.html Last accessed: 29th August, 2012.

Petrovsky, E., 2007. Susceptibility, in: Gubbins, D., Herrero-Bervera, E. (Eds.), *Encyclopedia of Geomagnetism and Paleomagnetism*. Springer, Netherlands, pp. 931-932.

Pullaiah, G., Irving, E., Buchan, K.L., & Dunlop, D.J., 1975. Magnetization changes caused by burial and uplift. *Earth and Planetary Science Letters* 28, 133-143.

Rice, P. M., 2005. *Pottery Analysis: A Sourcebook*. University of Chicago Press, IL.

Rusakov, O.M., Zagniy, G.F., 1973. Intensity of the geomagnetic field in the Ukraine and Moldavia during the past 6000 years. *Archaeometry* 15, 275-185.

Shaar, R., Ron, H., Tauxe, L., Kessel, R., Agnon, A., Ben-Yosef, E., Feinberg, J.M., 2010. Testing the accuracy of absolute intensity estimates of the ancient geomagnetic field using copper slag material. *Earth and Planetary Science Letters* 290, 201-213.

Sternberg, R.S., 2008. Archaeomagnetism in *Archaeometry*: a semi-centennial review. *Archaeometry* 50, 6, 983-998.

Sternberg, R.S., 2001. Magnetic properties and archaeomagnetism, in: Brothwell, D.R., Pollard, A.M. (Eds.), *Handbook of archaeological sciences*. John Wiley, Chichester, pp. 73–79.

Sternberg, R.S., 1992, Radiocarbon fluctuations and the geomagnetic field, in: (eds. R. E. Taylor, A. Long and R. Kra) *Radiocarbon after four decades*, 93–116, Springer-Verlag, New York.

Sternberg, R.S., 1990. The geophysical basis of archaeomagnetic dating, in: Eighmy, J.L., Sternberg R.S. (Eds.), *Archaeomagnetic Dating.* University of Arizona Press, Tucson, pp. 6-32.

Sternberg, R.S., McGuire, R.H., 1990a. Techniques for constructing secular variation curves and for interpreting archaeomagnetic dates, in: Eighmy, J.L., Sternberg R.S. (Eds.), *Archaeomagnetic Dating.* University of Arizona Press, Tucson, pp. 109–134.

Sternberg, R.S., McGuire, R.H., 1990b. Archaeomagnetic Secular Variation in the American Southwest, A.D. 700-1450, in: Eighmy, J.L., Sternberg R.S. (Eds.), *Archaeomagnetic Dating.* University of Arizona Press, Tucson, pp. 199-225.

Tanguy, J.C., 1970. An Archaeomagnetic study of Mount Etna: the magnetic direction recorded in lava flows subsequent to the twelfth century. *Archaeometry* 12, 115-128.

Tauxe, L., 2010. *Essentials of Paleomagnetism: Web Edition.* University of California Press. http://magician.ucsd.edu/Essentials/index.html

Tauxe, L., Staudigel, H., 2004. Strength of the geomagnetic field in the cretaceous normal superchron: new data from submarine basaltic glass of hetroodosophiolite. *Geochemistry, Geophysics. Geosystems* 5, 2, doi:10.1029/2003GC000635.

Tema, E., 2009. Estimate of the magnetic anisotropy effect on the archaeomagnetic inclination of ancient bricks. *Physics of the Earth and Planetary Interiors* 176, 213-223.

Thellier, E., Thellier, O., 1959. Sur l'intensité du champ magnétique terrestre dans le passé historique et géologique. *Annales de Geophysique* 15, 285–378.

Thompson, R., Aitken, M.J., Gibbard, P.L., Wymer, J.J., 1974. Paleomagnetic study of the Hoxnian lacustrine sediments. *Archaeometry* 16, 2, 223-245.

Watson, D., 1990. The intensity of the geomagnetic field in the eastern Mediterranean between 1600 BC and AD 400. *Geomagnetism and Geoelectricity* 42, 929-936.

Weaver, G. H., 1966. Measurement of the past intensity of the Earth's magnetic field. *Archaeometry* 9, 174-186.

Yu, J. H., 1990. Some thermal magnetic qualities of baked clay, in Eighmy, J.L., Sternberg, R.S. (Eds.), *Archaeomagnetic Dating.* University of Arizona Press, Tucson, pp. 81-101.

Appendix A. Sample Selection and Photos

Table A1. Details of Pottery Sample Selection

Sample ID	Site Phase	Archaeological Date (BCE)	Sample Label	Firing	Visible Temper	Visible Pore Space	Ware Type	Color	Average Thickness
Unit A9									
9	6	1595-1200	A09q717-f257	O	C, S	M,S,R	FC	Buff	0.6 cm
13	5	1900-1595	A09q752-f278	O	B	F,S,R	FC	Red	0.9 cm
14	5	1900-1595	A09q752-f278	O	C, S, B	F,S,R	FC	Orange	0.8 cm
23	6	1595-1200	A09q783-f198	O	C, S	M,L,E	RC	Orange	0.8 cm
Unit A14									
32	4	2112-1900	A14q373-f137	O	C, S, P	M,L,E	RC	Orange[2]	2.0 cm
35	3	2240-2112	A14q377-f133	O	C	F,S,R	FC	Buff	1.0 cm
37	*	*	A14q379-f137	R	C	F,L,E	IM	Grey	0.8 cm
40	1	2334-2270	A14q389-f193/143	R[1]	-	F,VL,E	S	Green	0.5 cm
51	4b	2000-1900	A14q403-f152	O	C, S	M,L,E	RC	Orange	1.3 cm
54	7	1200-modern	A14q420-f172	R	-	None	IM	Grey	0.4 cm
56	1	2334-2270	A14q474-f193	O	-	None	S	Greenish Buff	0.7 cm
58	7	1200-modern	A14q589-f221	O	C, B	VF,S,E	BR	Red[3]	0.8 cm
64	3	2240-2112	A14q649-f256	O	C, S	M,L,R,E	FC	Buff	1.0 cm
65	3	2240-2112	A14q649-f256	O	C	M,S,R	FC	Buff	0.6 cm

72	4	2112-1900	A14q761-f124	O	C, S	M,L,E	RC	Red	1.0 cm
Unit A16									
mds01	3b/4	2192-2004	A16q780-f289	O	C, S, M, B	M,S,R	FC	Orange	0.8 cm
mds04	3b/4	2192-2004	A16q841-f289	O	C, S	M,S,R	FC	Buff	0.4 cm

Pottery samples chosen for testing were either fully oxidized (O) or reduced (R) but high fired. Any visible temper inclusions, as identified by hand lens prior to testing, are listed as calcareous (C), sand (S), mica (M), iron oxide (I), and unknown black mineral (B). Visible pore spaces were many (M), few (F), very few (VF), small (S), large (L) or very large (VL), rounded (R) or elongated/irregular (E). Unidentifiable elements are not listed. Probable manufacture process is listed if identifiable. Ware Types: FC = Fine Chaff, RC = Red-Orange Calcite, IM = Imitation Metal, S = Sand, BR = Burnt Red Ware.

[1] Sample 40 had a faint carbon core

[2] Sample 32 had an orange exterior, red interior

[3] Sample 58 had a red exterior, orange interior

** Samples 37 had no known phase association from the Tell Mozan database*

Figure A1. Photos of All Samples Prior to Preparation

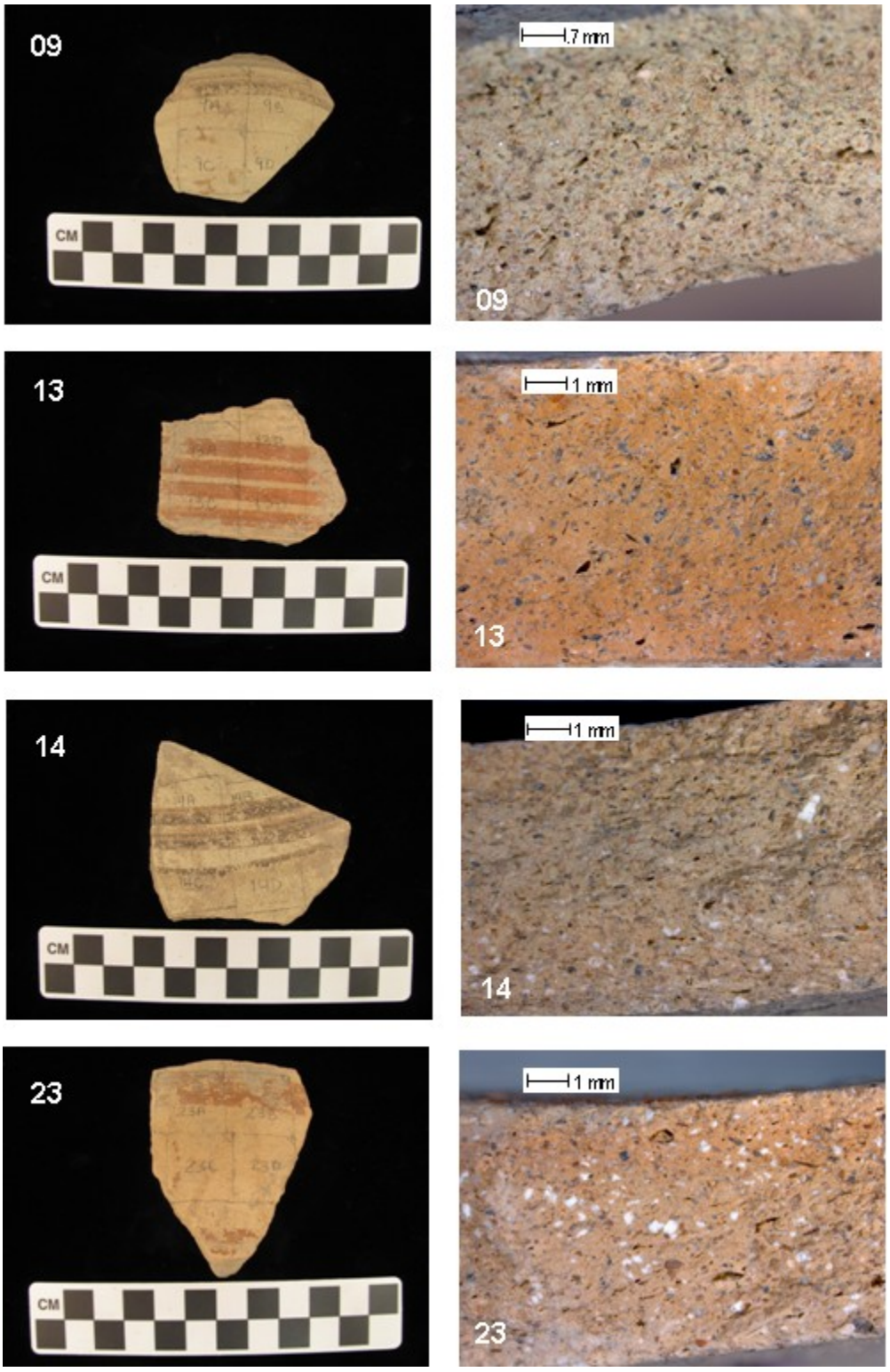

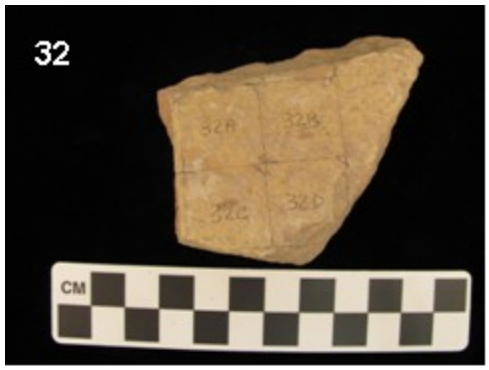
32
CM

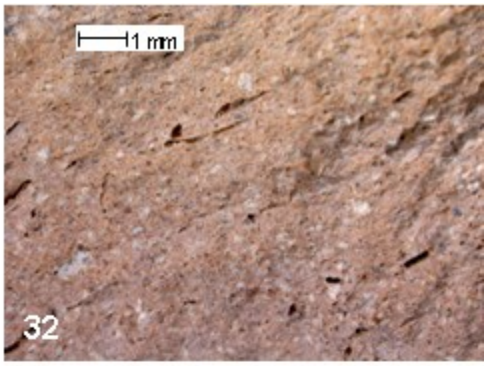
1 mm
32

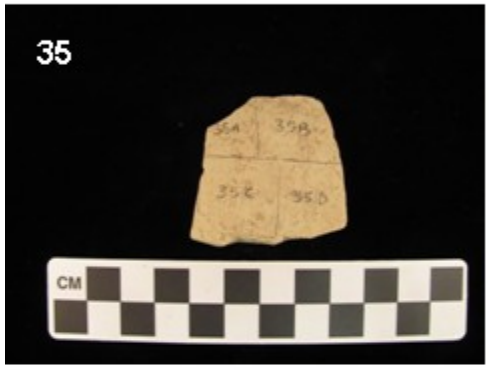
35
CM

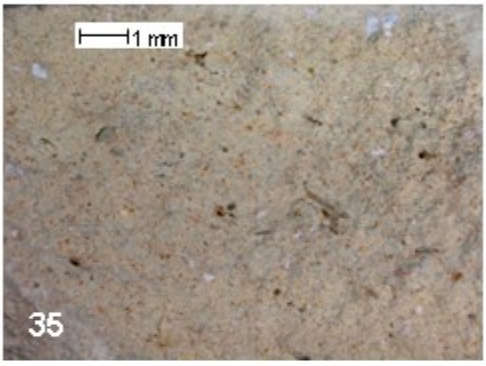
1 mm
35

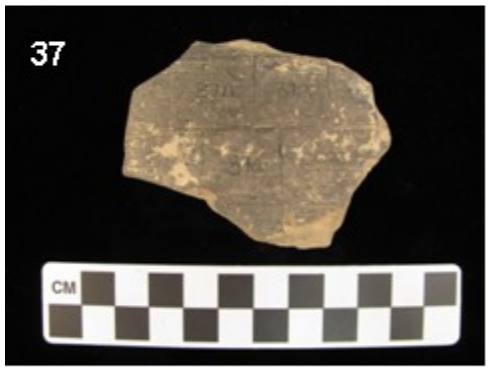
37
CM

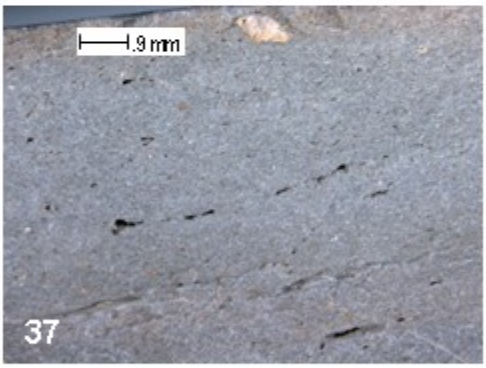
.9 mm
37


40
CM

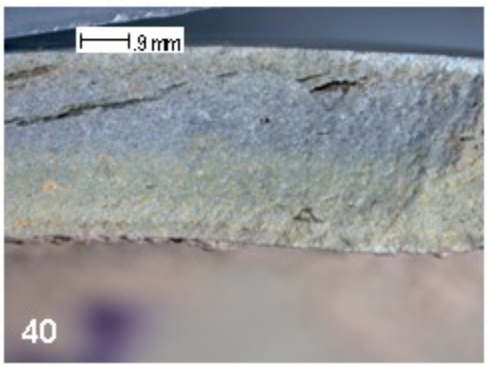
.9 mm
40


51
CM


1 mm
51


54
CM

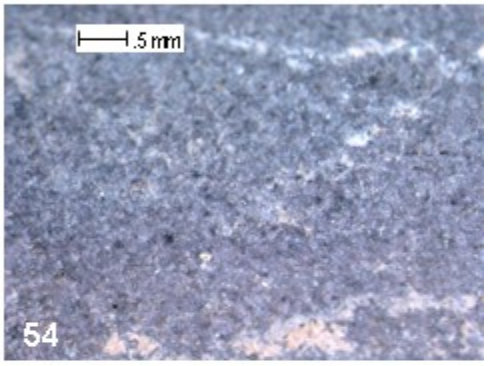
.5 mm
54


56
CM

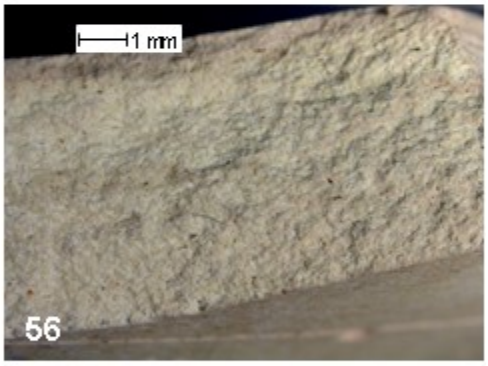
1 mm
56

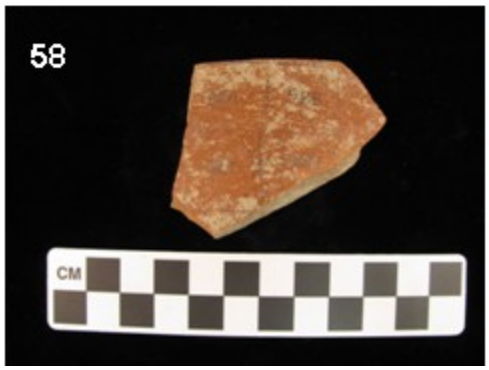
58
CM

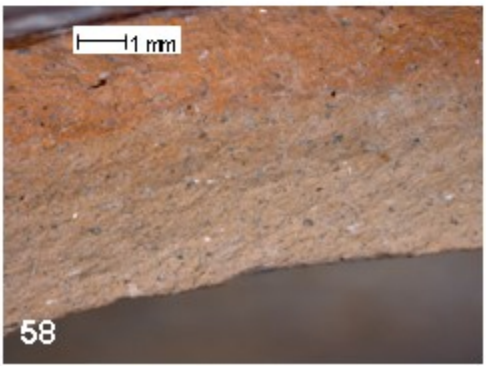
1 mm
58

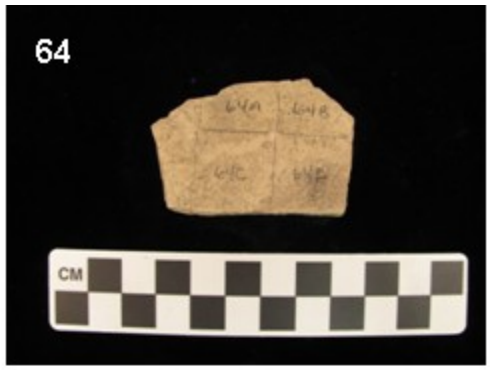
64
CM


1 mm
64


65
CM

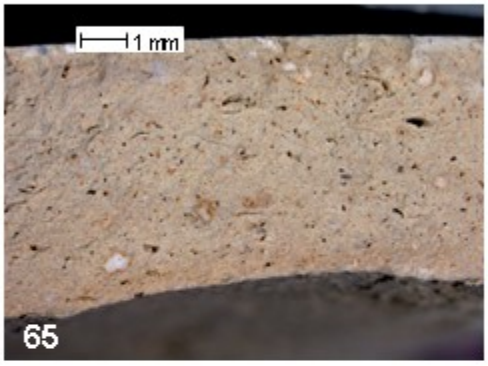
1 mm
65


72
CM

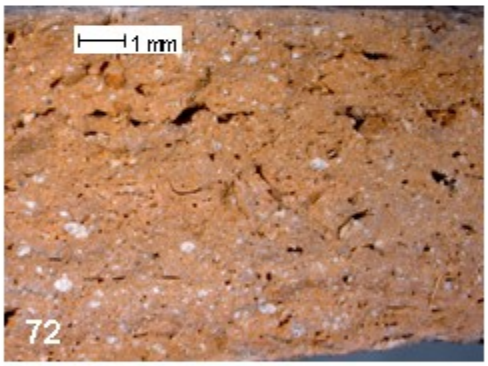
1 mm
72


mds01
CM

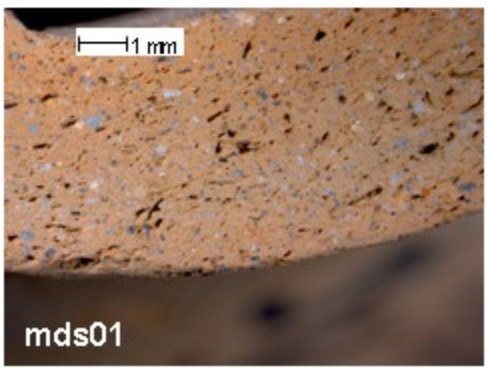
1 mm
mds01

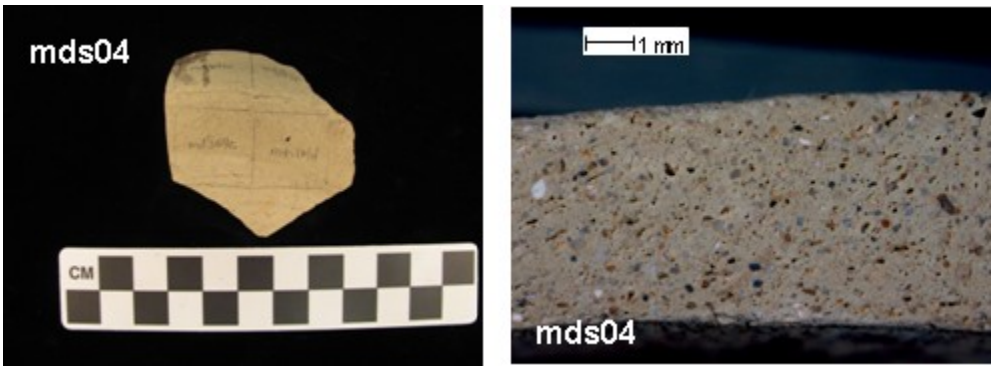

Cores photographed using a Leica MZ16A Microscope.

Appendix B. All Sample Results and Curve Construction Parameters

Table B1. Results of Susceptibility, Hysteresis, and AF Demagnetization

Sample ID	Average χ (m^3/kg)	χ_{lf} (m^3/kg)	χ_{hf} (m^3/kg)	χ_{fd} (%)	Ms (Am^2/kg)	Mr (Am^2/kg)	Hc (mT)	Hcr (mT)	NRM (Am^2/kg)	MDF (mT)
09	3.50E-06	2.92E-06	2.80E-06	3.93	1.56E-01	5.69E-02	17.6	32.3	3.05E-03	27.6
13	4.31E-06	4.15E-06	3.74E-06	9.98	1.38E-01	2.66E-02	8.3	21.1	1.37E-03	9.4
14	3.99E-06	4.05E-06	3.71E-06	8.39	1.48E-01	4.51E-02	12.0	28.5	1.36E-03	25.0
23	4.86E-06	4.96E-06	4.50E-06	9.13	1.57E-01	3.01E-02	7.4	16.5	2.42E-03	14.6
32	5.47E-06	5.75E-06	5.19E-06	9.81	2.59E-01	7.48E-02	11.6	29.5	3.05E-03	15.4
35	3.65E-06	3.70E-06	3.55E-06	4.02	4.33E-01	1.12E-01	6.6	12.9	2.65E-03	11.2
37	8.53E-07	9.97E-07	9.44E-07	5.31	5.53E-02	1.14E-02	14.2	32.0	3.35E-04	9.5
40	2.26E-07	2.11E-07	2.08E-07	1.63	1.39E-02	3.17E-03	7.8	22.1	1.28E-04	15.6
51	1.95E-06	2.16E-06	1.90E-06	11.97	3.83E-02	4.44E-03	3.7	15.2	1.98E-04	18.5
54	2.01E-06	1.87E-06	1.85E-06	1.08	1.95E-01	6.22E-02	25.4	44.8	3.99E-03	52.7
56	4.18E-07	4.07E-07	3.97E-07	2.30	1.42E-02	5.33E-03	16.1	28.7	3.85E-04	11.2
58	4.37E-06	4.49E-06	4.05E-06	9.86	1.34E-01	2.38E-02	6.6	15.9	1.96E-03	7.7
64	5.65E-06	5.54E-06	5.22E-06	5.81	1.67E-01	4.55E-02	6.6	11.8	1.37E-02	10.0
65	4.11E-06	4.13E-06	3.86E-06	6.54	1.10E-01	3.25E-02	7.9	16.1	3.01E-03	14.8

72	6.45E-06	6.79E-06	6.13E-06	9.68	2.18E-01	2.51E-02	4.4	14.4	9.15E-04	7.0
mds01	6.11E-06	6.08E-06	5.46E-06	10.22	1.84E-01	3.52E-02	7.2	19.1	1.25E-03	7.5
mds04	2.48E-06	2.42E-06	2.25E-06	6.80	8.26E-02	2.68E-02	13.6	33.2	1.19E-03	25.1

Susceptibility (χ) is average for all three specimens in the sample, all remaining results based on measurements obtained from one of three specimen sets. χ_{lf} is low frequency susceptibility, χ_{hf} is high frequency susceptibility, χ_{fd} is frequency dependence of susceptibility, Ms is saturation magnetization, Mr is remanent magnetization, Hc is coercivity, Hcr is coercivity of remanence, NRM is natural remanent magnetization, and MDF is median destructive field.

Table B2. Additional Details from Intensity Experiments and Acceptance Test Results

Specimen	T min (°C)	T max (°C)	n	b	Beta β	q	f	f_{vds}	gap g	sigma	DANG (°)	DRATS (%)	MD (%)	MAD (°)	Susc. χ [1]	DANG test <5	f test >0.6	MAD test <8
9a	200	550	13	-1.059	0.017	48.1	0.878	0.831	0.906	0.018	0.2	19.3	0.6	1.9	4.06	Good	Good	Good
13a	225	600	13	-1.410	0.020	35.9	0.812	0.787	0.869	0.028	0.2	56.1	0.4	3.2	4.40	Good	Good	Good
14a	225	550	12	-1.319	0.039	14.8	0.650	0.750	0.898	0.052	3.2	25.2	0.6	7.3	3.91	Good	Good	Good
23a	100	550	17	-1.483	0.025	32.9	0.902	0.680	0.928	0.038	0.2	17.0	0.8	1.7	4.90	Good	Good	Good
32a	175	550	14	-1.693	0.027	26.9	0.808	0.679	0.903	0.046	0.5	30.8	0.8	2.7	5.48	Good	Good	Good
35c	125	500	15	-1.608	0.014	54.5	0.885	0.669	0.886	0.023	0.1	19.7	0.5	1.8	3.63	Good	Good	Good
37a	***225***	***450***	***10***	***-1.485***	***0.053***	***5.6***	***0.339***	***0.425***	***0.883***	***0.079***	***6.2***	***56.3***	***0.3***	***11.9***	***0.81***	***Fail***	***Fail***	***Fail***
40a	175	600	15	-1.588	0.035	22.8	0.865	0.710	0.918	0.055	1.4	16.6	0.6	3.4	0.23	Good	Good	Good
51a	175	600	15	-1.735	0.029	19.9	0.620	0.609	0.922	0.050	1.7	7.7	1.4	3.2	1.91	Good	Good	Good
54a	300	500	8	-2.458	0.063	5.2	0.645	0.866	0.517	0.156	1.5	24.9	0.7	3.0	2.05	Good	Good	Good
56a	225	550	12	-1.259	0.017	44.2	0.876	0.821	0.852	0.021	0.3	19.1	0.8	2.1	0.42	Good	Good	Good
58a	200	550	13	-1.583	0.028	22.5	0.713	0.719	0.896	0.045	1.6	41.6	0.7	3.2	4.22	Good	Good	Good
64c	***200***	***450***	***11***	***-2.601***	***0.082***	***7.6***	***0.707***	***0.311***	***0.877***	***0.213***	***10.8***	***33.0***	***0.4***	***6.9***	***5.75***	***Fail***	***Fail***	***Good***
65a	150	450	13	-1.298	0.018	40.8	0.835	0.644	0.893	0.024	0.4	19.6	0.5	2.2	4.03	Good	Good	Good
72a	125	500	15	-1.277	0.069	9.7	0.732	0.621	0.912	0.088	3.2	8.3	1.3	7.0	6.45	Good	Good	Good
mds01a	200	600	14	-1.578	0.022	25.8	0.636	0.654	0.910	0.035	1.1	19.9	0.9	7.9	6.15	Good	Good	Good
mds04a	175	600	15	-1.221	0.026	27.8	0.796	0.698	0.918	0.032	2.6	31.2	0.4	6.6	2.47	Good	Good	Good

The Tmin and Tmax represent min and max temperatures of best-fit line used in intensity calculations. n = number of measurements within that temperature range. b = value of the slope. Beta = sigma/slope. q = (b)(f)(gap)/sigma. f = fraction of NRM remanence used from arai plot. g = gap or spacing of the points along the slope (value of 1 is best). The Deviation Angle (DANG) is the angle between the best-fit line of the data and the best-fit line from the origin through the center of mass of the data. The Maximum Angular Deviation (MAD) represents the variance of the points within a particular temperature interval used to define the direction. The β is the scatter parameter of Coe et al. (1978). The Difference Ratio Sum (DRATS) indicate the sum of all pTRMs divided by the total pTRM incorporated by the best-fit straight line; and fvds is the fraction of magnetization normalized by the vector difference sum (vds) of the NRM used to calculate the slope of the line that defines the intensity. 1 Susceptibility χ = value x 10-6 m3/kg. Criteria for acceptance of sample results were set as follows: DANG test <5, f test >.06, MAD test <8. Sample 37a failed all three tests. Sample 64c failed DANG and f tests. Both samples were rejected.

Table B3. Intensity and ARM Results

Specimen	Archaeological Date (BCE)	Raw Ba (μT)	Ba AARM Corr (μT)	Ba error (μT)	VDM (ZAm^2)	err.VDM (ZAm^2)
58a	1200-modern	47.5	56.9	2.6	102.1	4.7
54a	1200-modern	73.7	85.8	13.4	154.0	24.1
9a	1595-1200	31.8	36.5	0.6	65.5	1.1
23a	1595-1200	44.5	49.5	1.9	88.9	3.4
14a	1900-1595	39.6	42.2	2.2	75.7	4.0
13a	1900-1595	42.3	43.9	1.2	78.8	2.2
51a	2000-1900	52.1	54.8	2.7	98.4	4.8
72a	2112-1900	38.3	42.3	3.7	75.9	6.6
32a	2112-1900	50.8	53.5	2.5	96.0	4.5
mds04a	2192-2004	36.6	39.6	1.3	71.1	2.3
mds01a	2192-2004	47.4	54.3	1.9	97.5	3.4
35c	2240-2112	48.2	49.6	1.1	89.0	2.0
65a	2240-2112	38.9	44.2	1.0	79.3	1.8
64c	2240-2112	78.0	72.9	15.6	130.9	28
40a	2334-2270	47.6	44.5	2.5	79.9	4.5
56a	2334-2270	37.8	44.5	0.9	79.9	1.6
37a	unknown	44.6	45.7	3.6	82.0	6.5

Ba is intensity in microTesla (μT), VDM is Virtual Dipole Moment in $Am^2 \times 10^{22} (ZAm^2)$

Table B4. Polynomials Used in Construction of Best-fit Line for Intensity Curves

Polynomial Order	Polynomial Coefficient	Value (Fig. 12)	Value (Fig. 13)	Value (Fig. 14)
x9	a	1.5041×10^{-26}	7.8421×10^{-28}	9.5222 x 10-38
x8	b	2.2144×10^{-22}	1.4854×10^{-23}	1.7692 x 10-23
x7	c	1.3740×10^{-18}	1.1628×10^{-19}	1.3595 x 10-19
x6	d	4.6538×10^{-15}	4.8350×10^{-16}	5.5546 x 10-16
x5	e	9.2947×10^{-12}	1.1399×10^{-12}	1.2885 x 10-12
x4	f	1.0998×10^{-8}	1.5004×10^{-9}	1.6717 x 10-9
x3	g	7.3220×10^{-6}	1.0068×10^{-6}	1.1080 x 10-6
x2	h	0.0024	0.0003	0.0003
x	i	0.3292	0.03671	0.03761
Constant	j	43.4608	51.9774	52.0762